Surface effects in hyperspectral infrared measurements from the AIRS instrument of the Aqua satellite

(Experimental Processing of IR Measurements from the AIRS Instrument)

Youri Plokhenko[#] , W. Paul Menzel[&]

[#] CIMSS, University of Wisconsin – Madison
[&] Office of Research and Applications , NOAA/ NESDIS

The importance of **incorporating the surface emissivity in the solution** of the atmospheric infrared remote sensing inverse problem is explained by:

* **Optically "black" surfaces don't exist**; emissivity variations cause measurable changes in infrared radiance

* Satellite meteorological **remote sensing instruments have good radiometric sensitivity** with a relative accuracy of .2K. Disregarding the spectral-spatial variations of emissivity in the radiative transfer model (in the atmospheric windows) magnifies the errors by at least a factor of three to five.

* To realize the potential of the satellite measurements, **a radiative transfer model accounting for surface emissivity must be used**.

* Different kinds of surface cover, with different surface optical properties, with extremely high spatial and temporal variations, restrict the use of a priori estimates of the surface effects. The **direct evaluation of emissivity in the inverse solution is** a simpler and more **effective approach**.

AIRS over Europe on 6 Sep 02

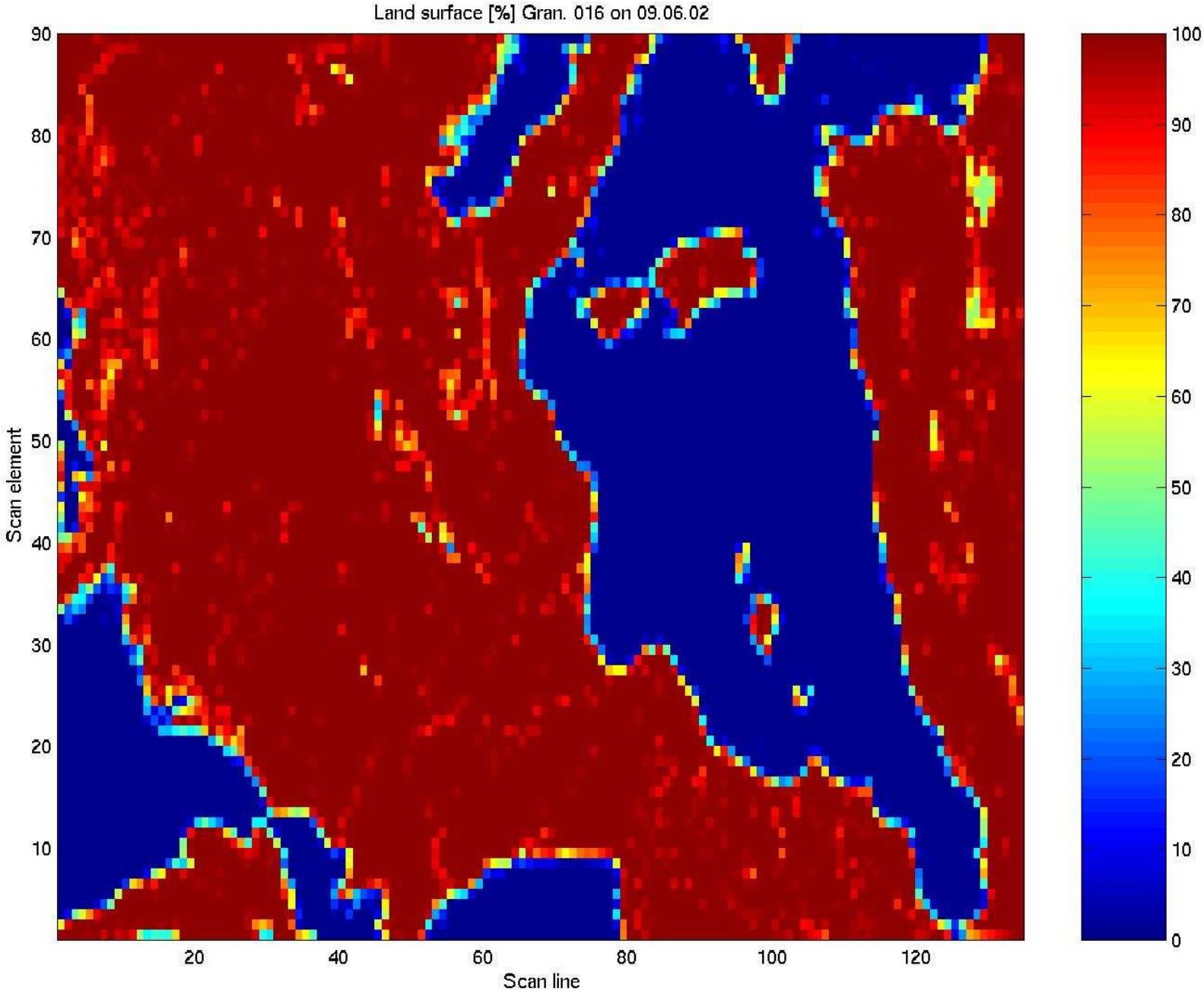

Spatial distribution of Ch 1552 at 1385.02 [1/cm] measurements [K]

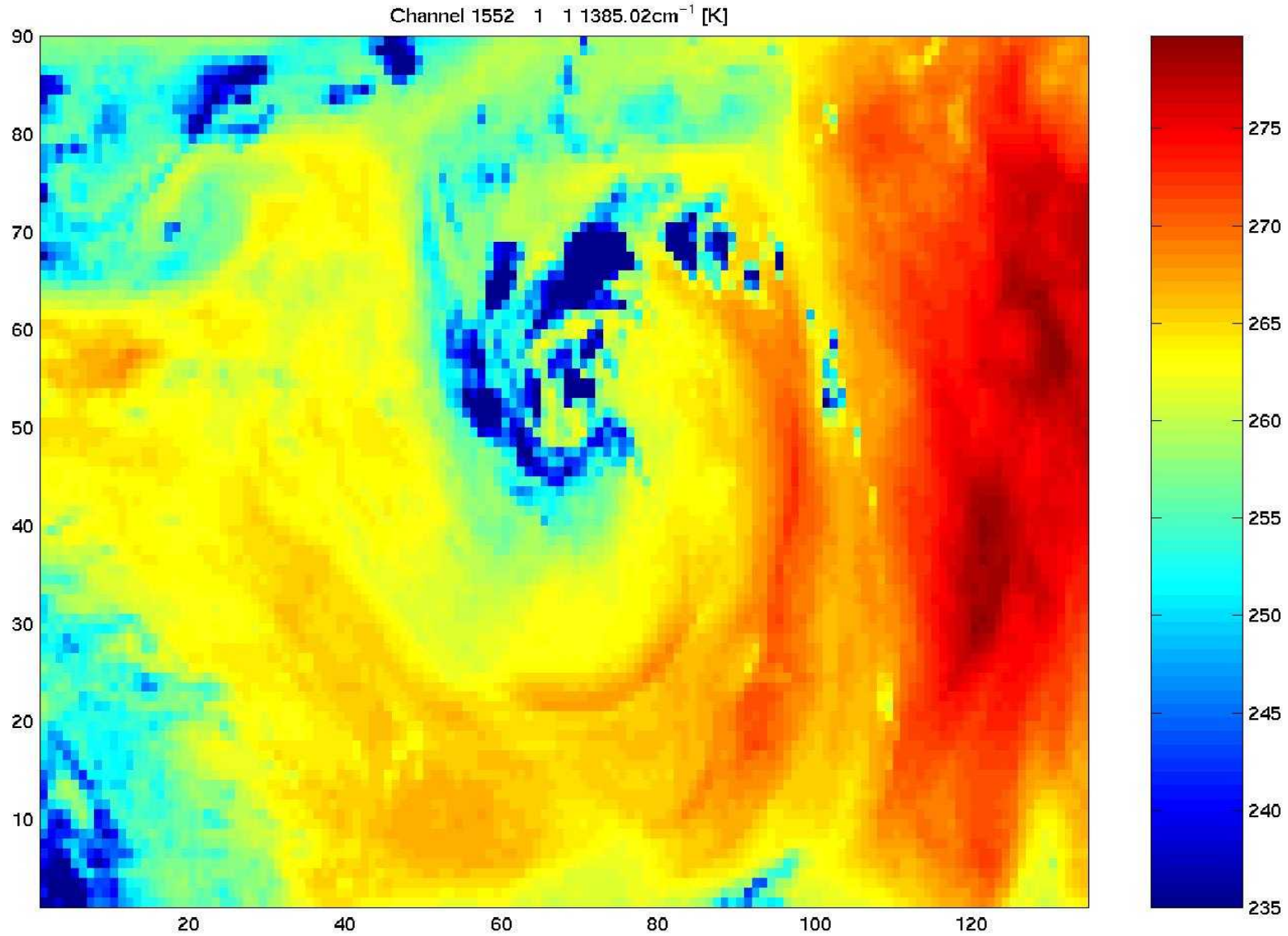

Spatial distribution of Ch 1553 at 1385.57 [1/cm] measurements [K]

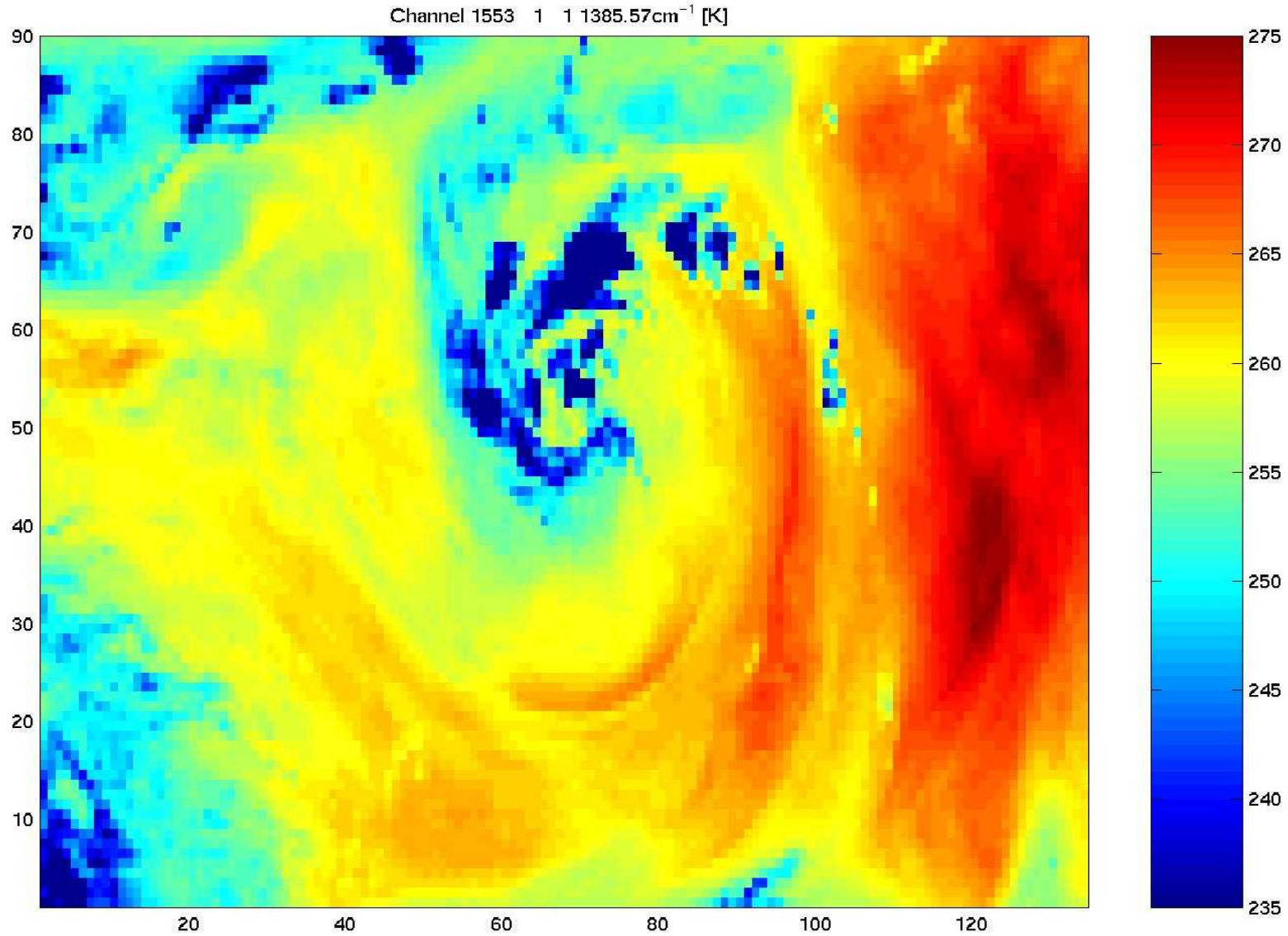

Spatial distribution of Ch 1554 at 1386.11 [1/cm] measurements [K]

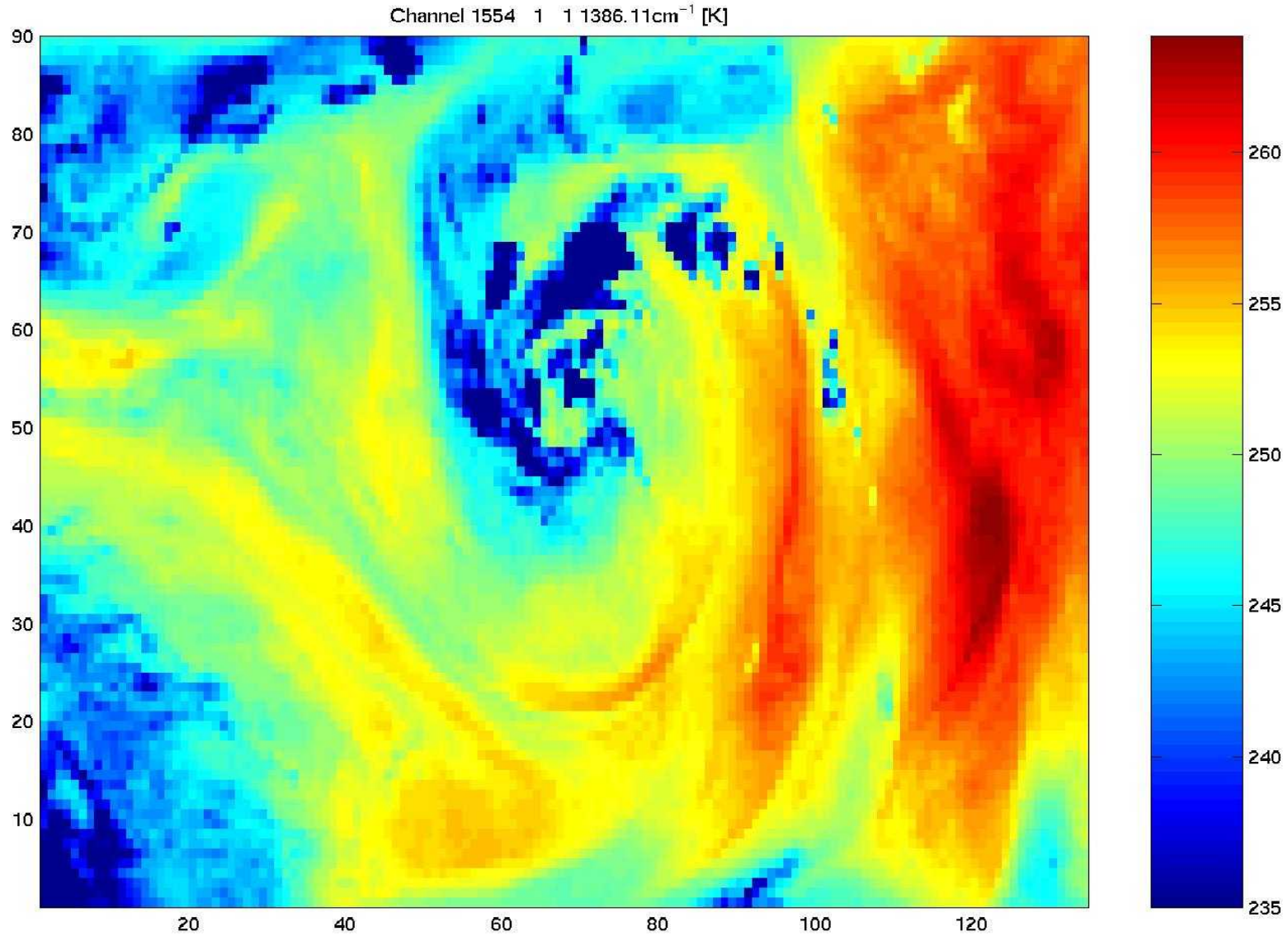

Spatial distribution of Ch 1555 at 1386.66 [1/cm] measurements [K]

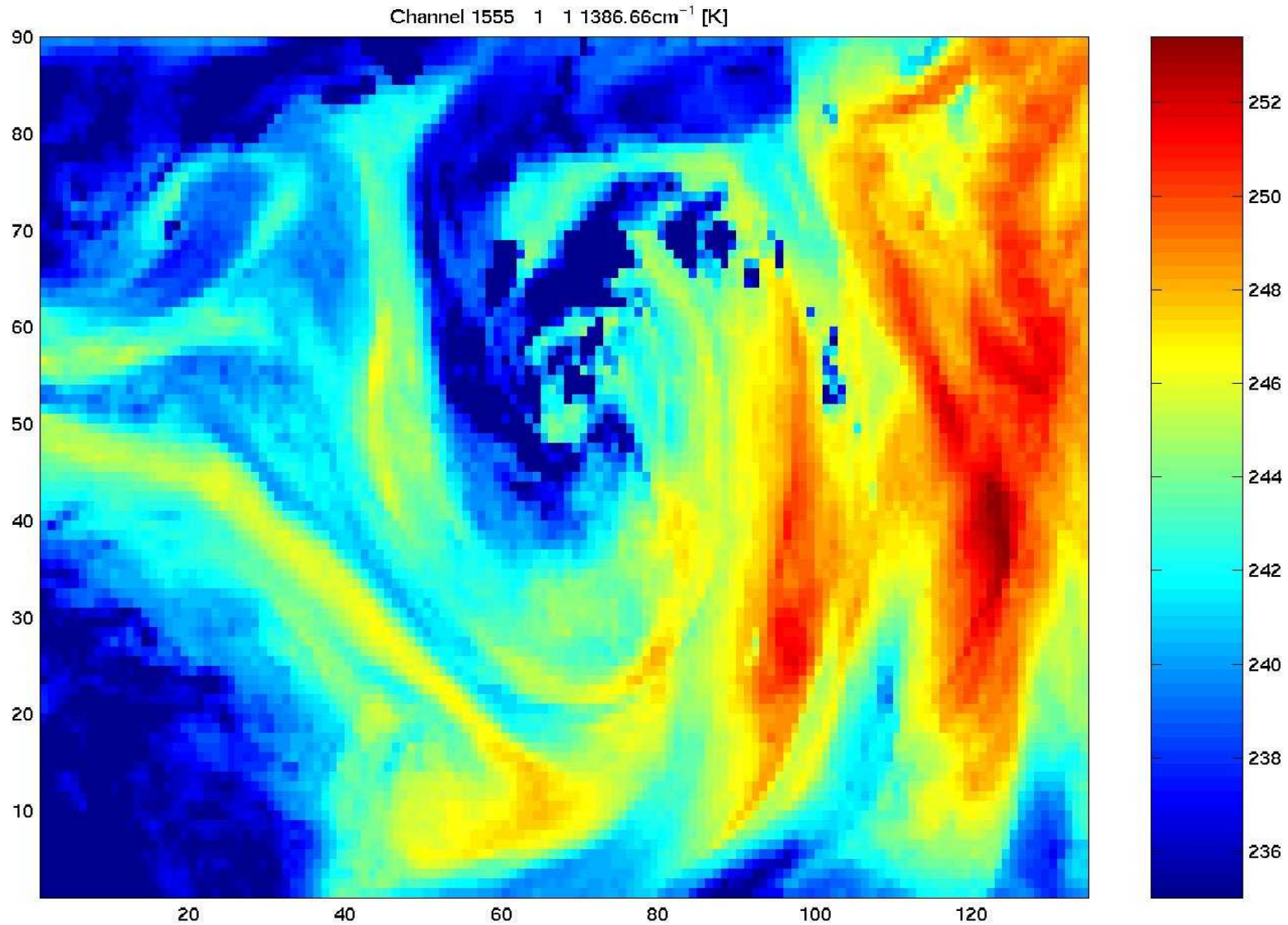

Spatial distribution of Ch 1556 at 1387.21 [1/cm] measurements [K]

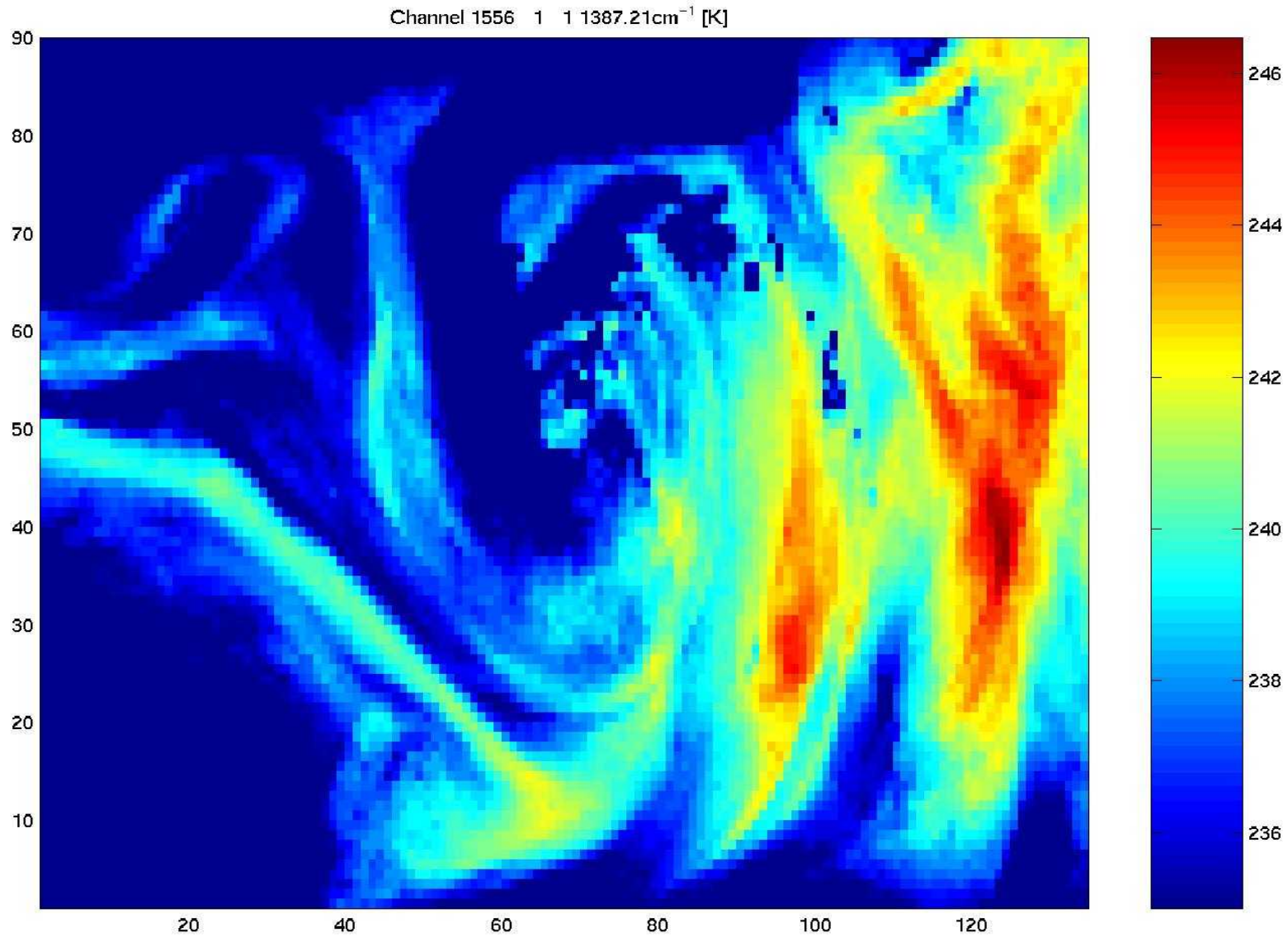

AIRS radiance changes (in deg K) to atm & sfc changes

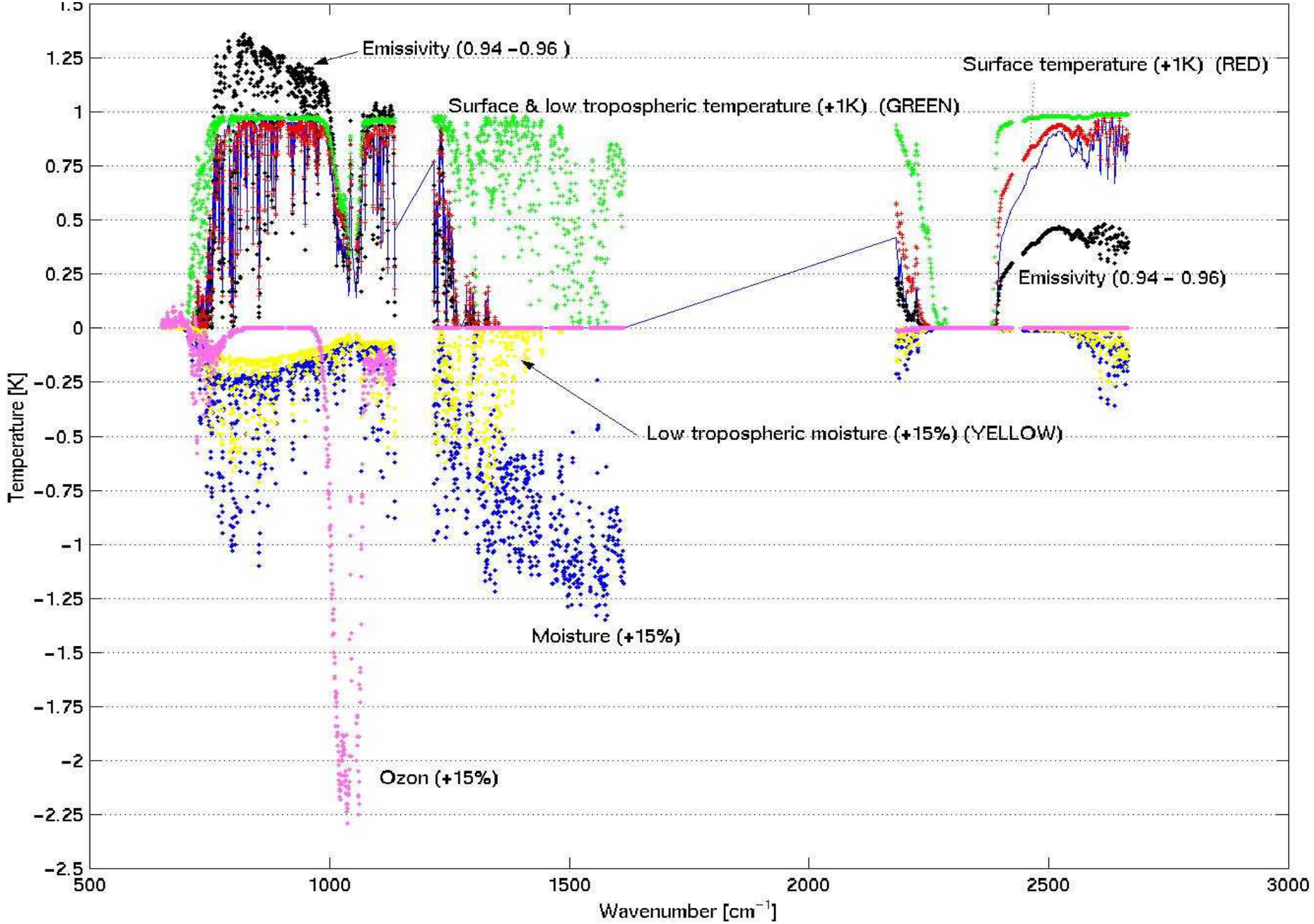

Optical properties of cloud particles: imaginary part of refraction index

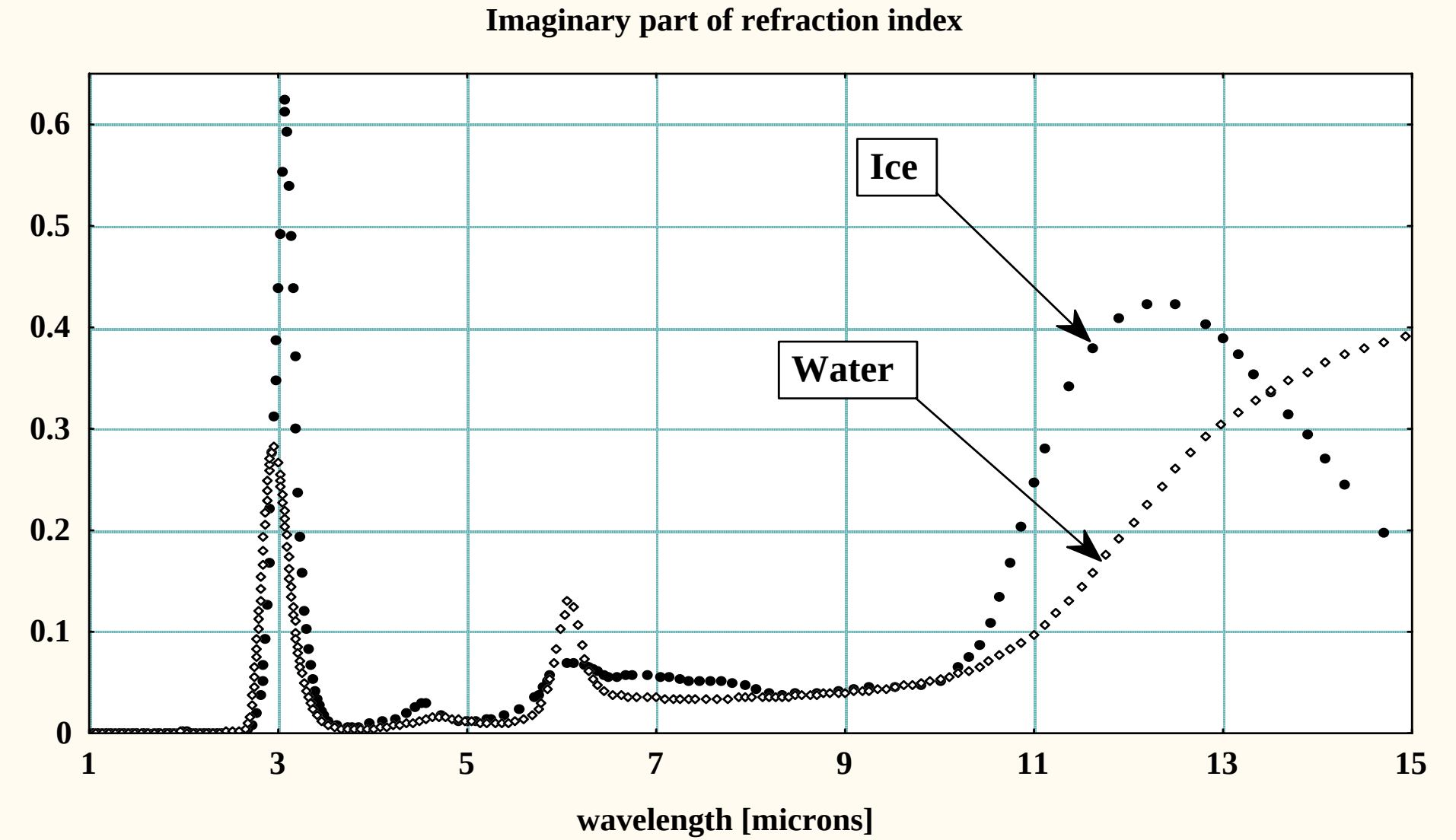

SW & LW channel differences are used for cloud identification
{4 μm - 11μm}, {4.13 μm - 12.6μm}, and {4.53 μm - 13.4μm}

Spatial distribution of 944.1 [1/cm] measurements [K]

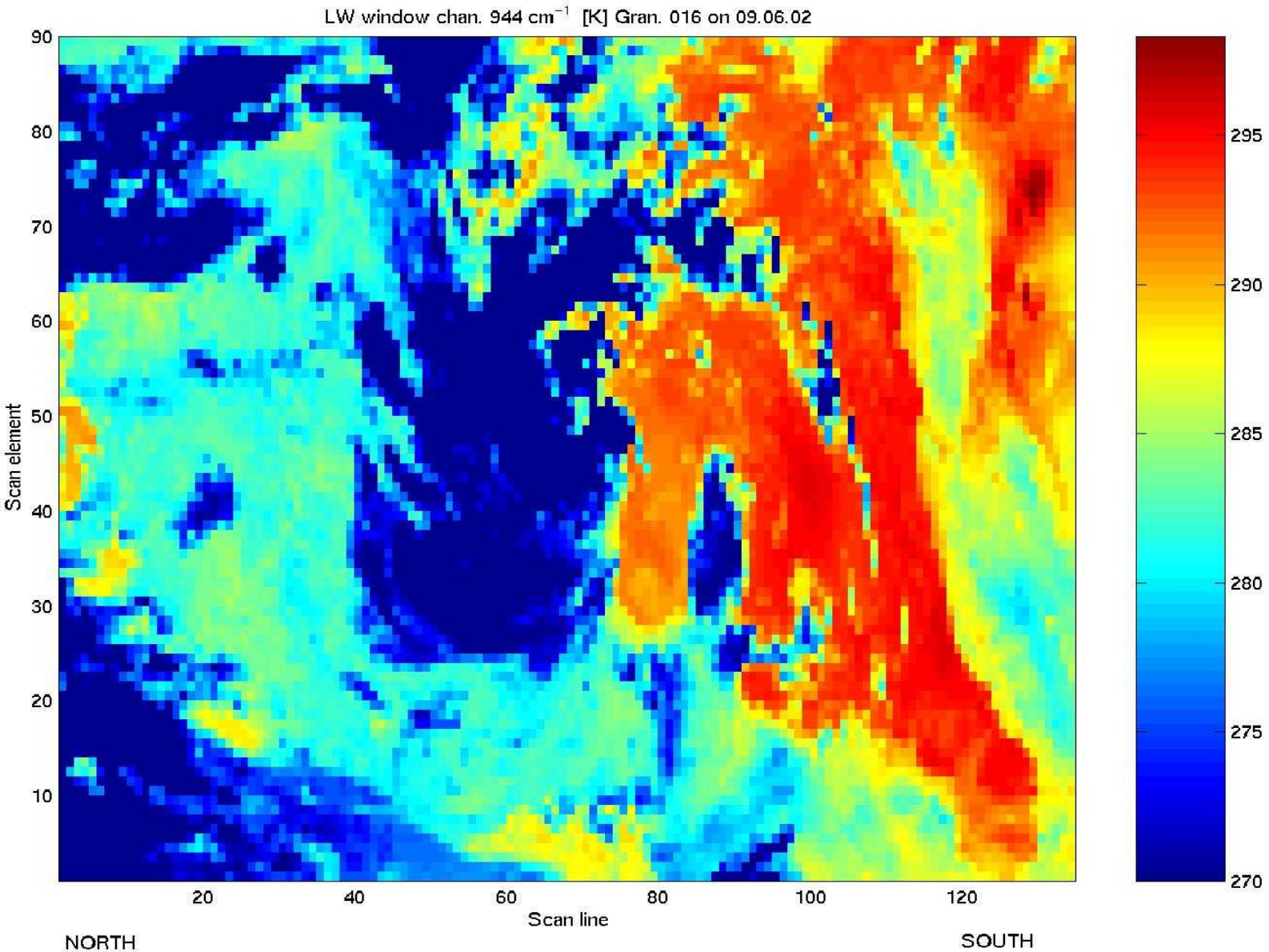

Spatial distribution of 2555 [1/cm] measurements [K]

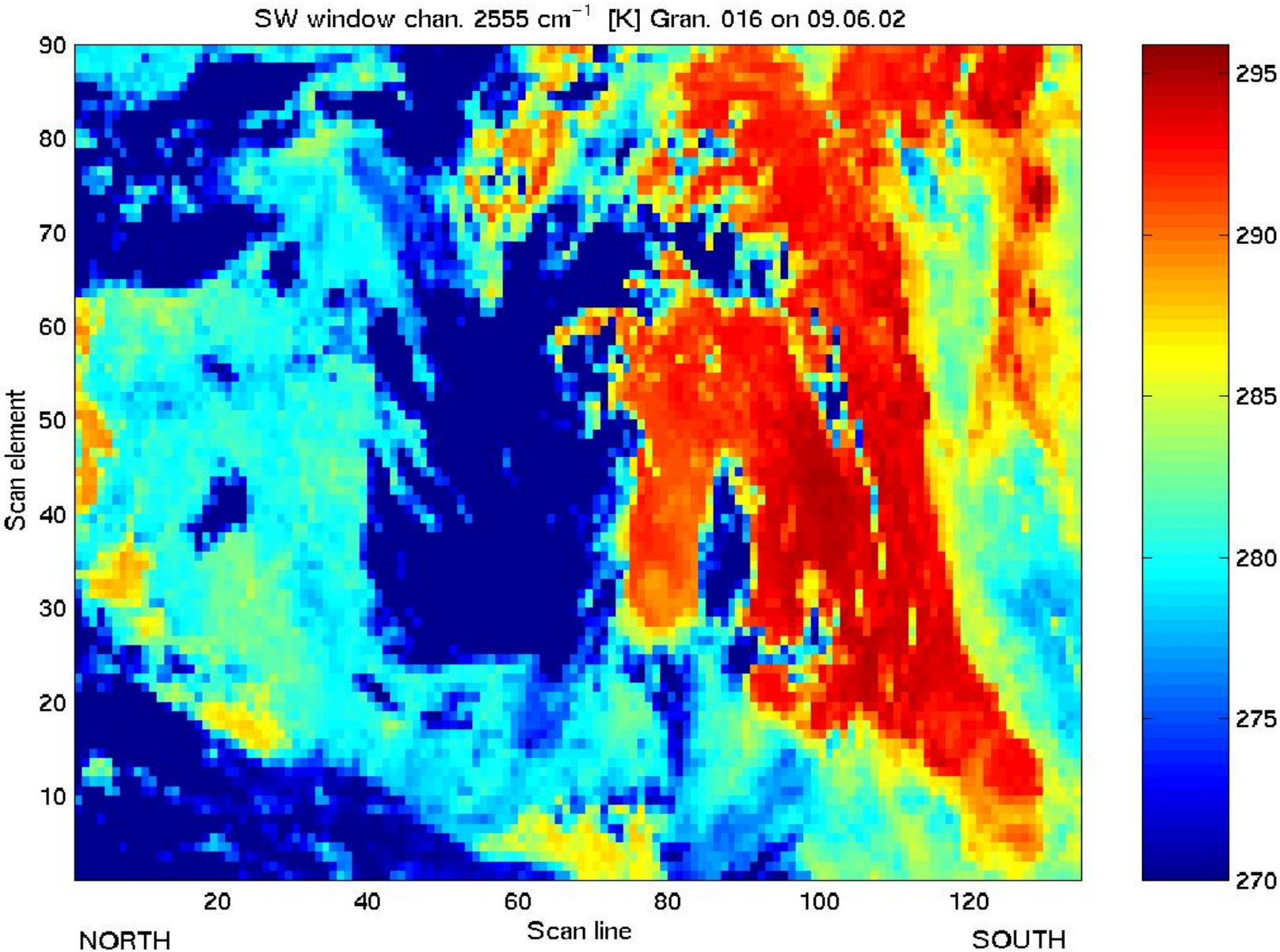

Spatial distribution of 2555 – 944.1 [1/cm] measurements [K]

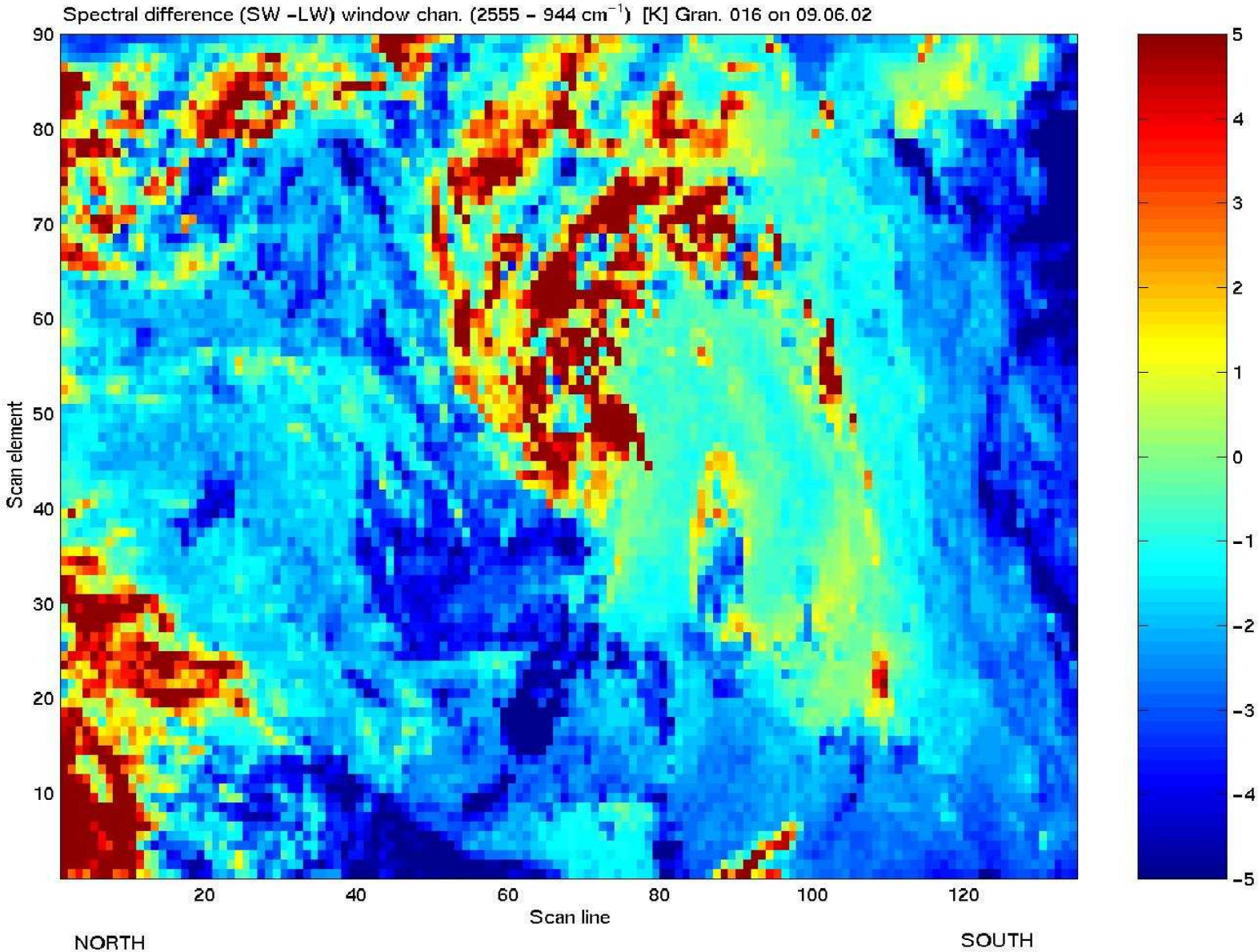

1 - StDev of bb measurement error [K] (RED), 2 - StDev of earth measurements [K] (BLUE); 3 - total atmospheric transmittance

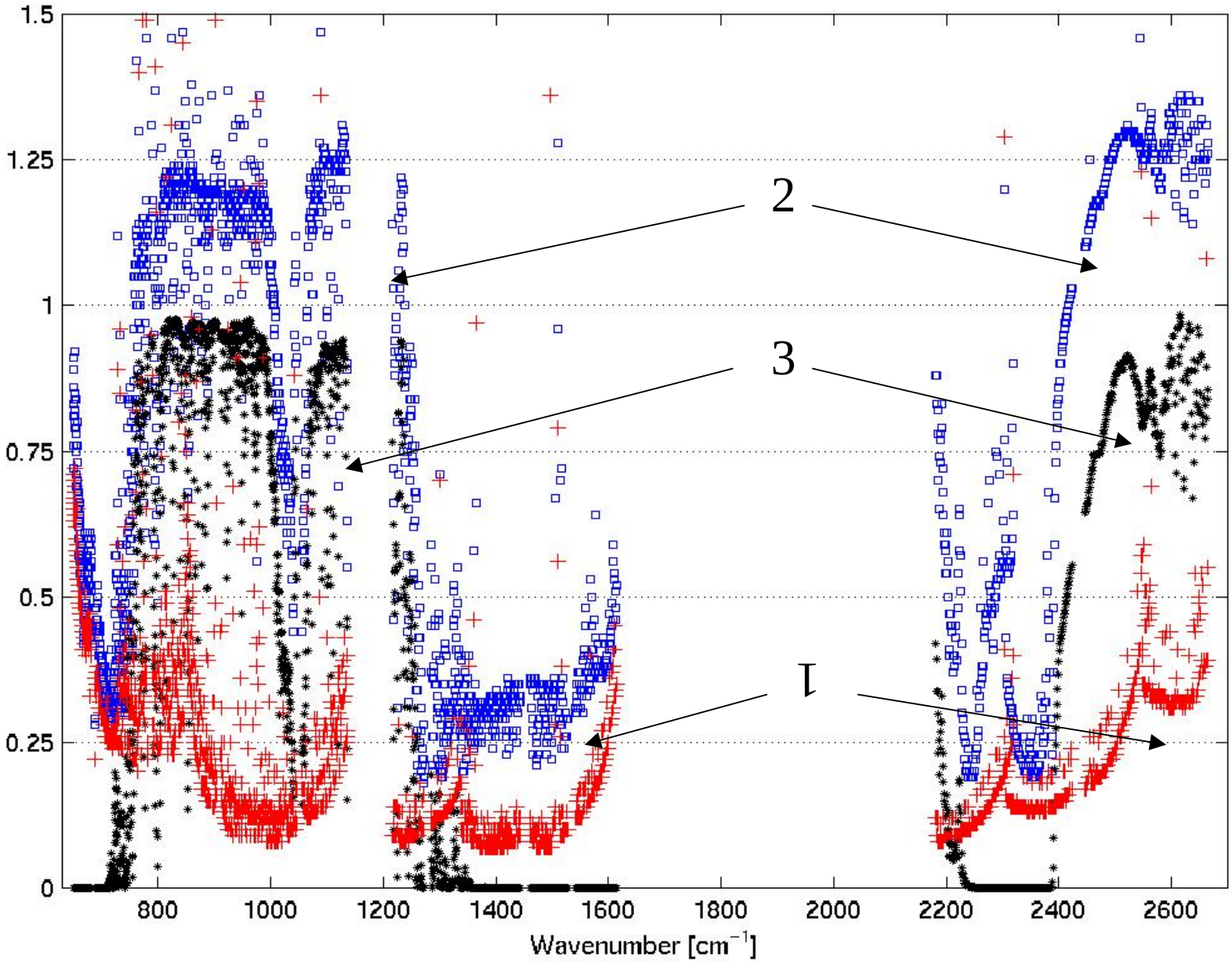

The following issues are addressed:

* to improve the signal to noise ratio, a spatial filtering procedure is developed; spatial smoothing is used in all spectral channels (a rectangular box of variable size defined for each spectral band is used for each field of view);

* to identify the presence of cloud, tests for spatial smoothness (second differential), and spectral smoothness (differences between LW band channels and SW band channels) are used;

* spatial averaging and cloud identification are combined in a joint algorithm for data analysis: averaging $\mapsto$ identification $\mapsto$ averaging on “clear” sub-sample;

* the temporal-spatial structure of errors is discussed, and the shortwave and longwave components of the errors are estimated.

Spectral distribution of spatial smoothing filter

(half-size given in pixel number)

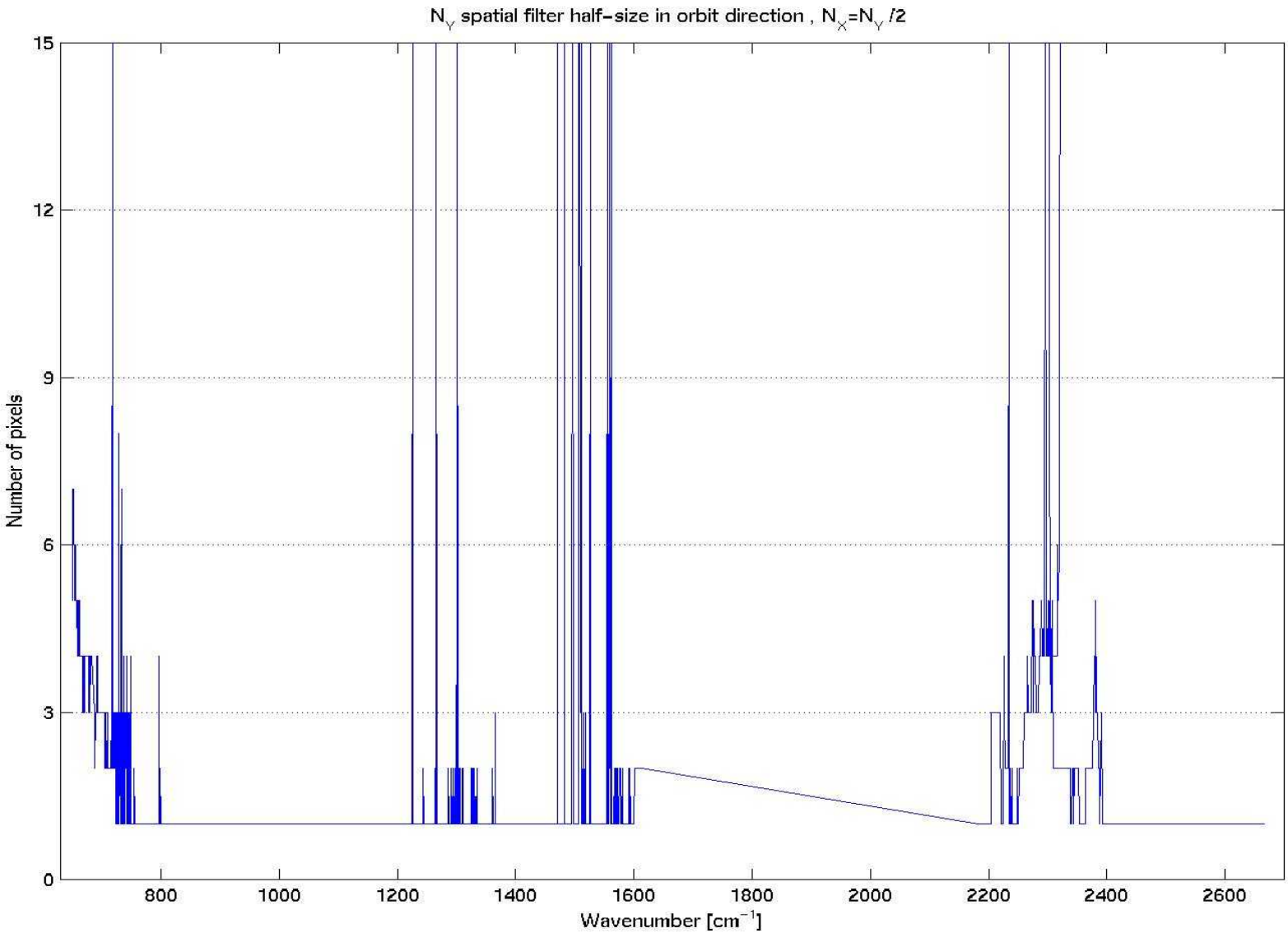

Spatial distribution of Ch 121 at 679.62 [1/cm] measurements [K]

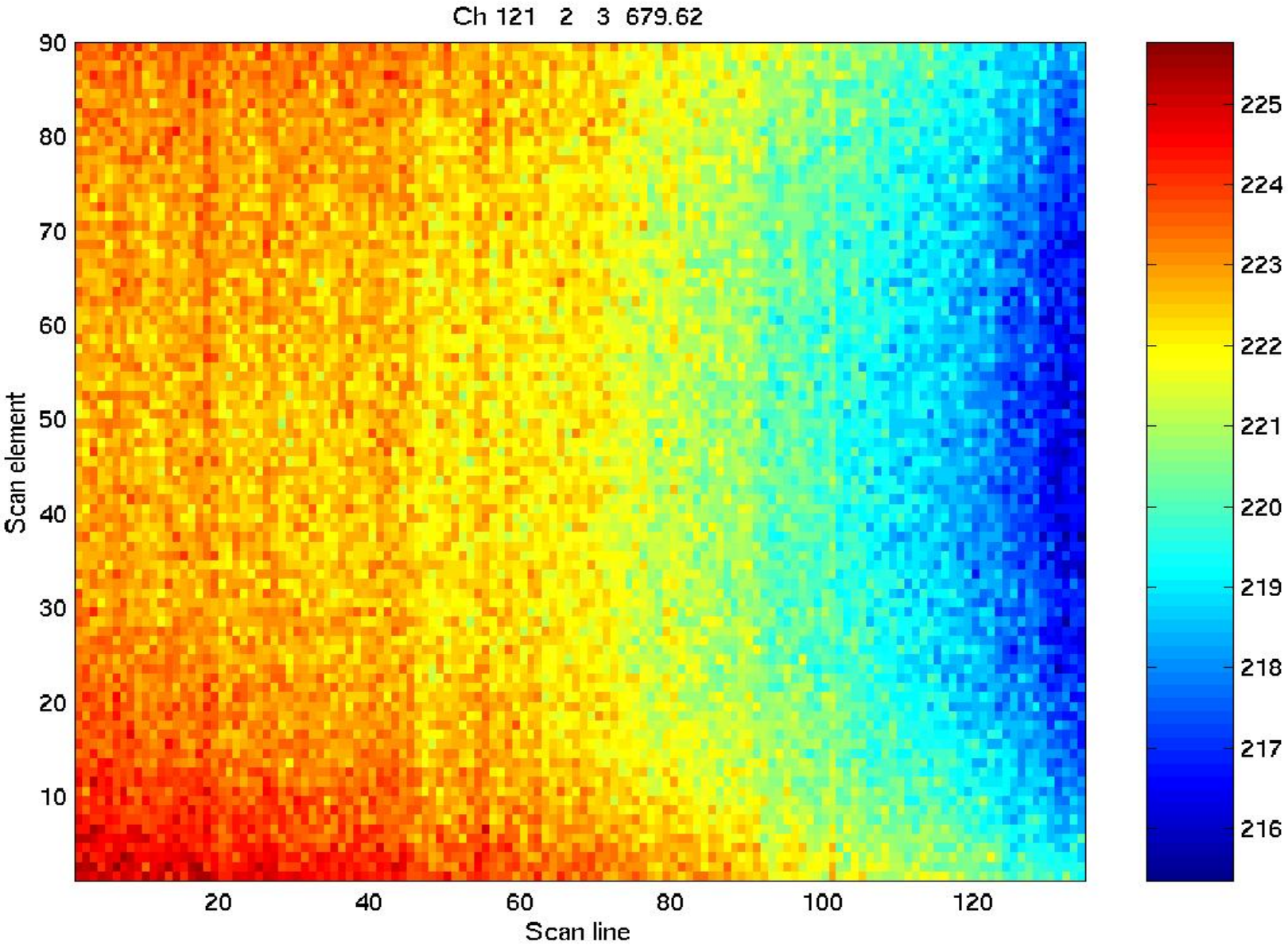

Spatial distribution of Ch 121 at 679.62 [1/cm] measurements [K] filtered

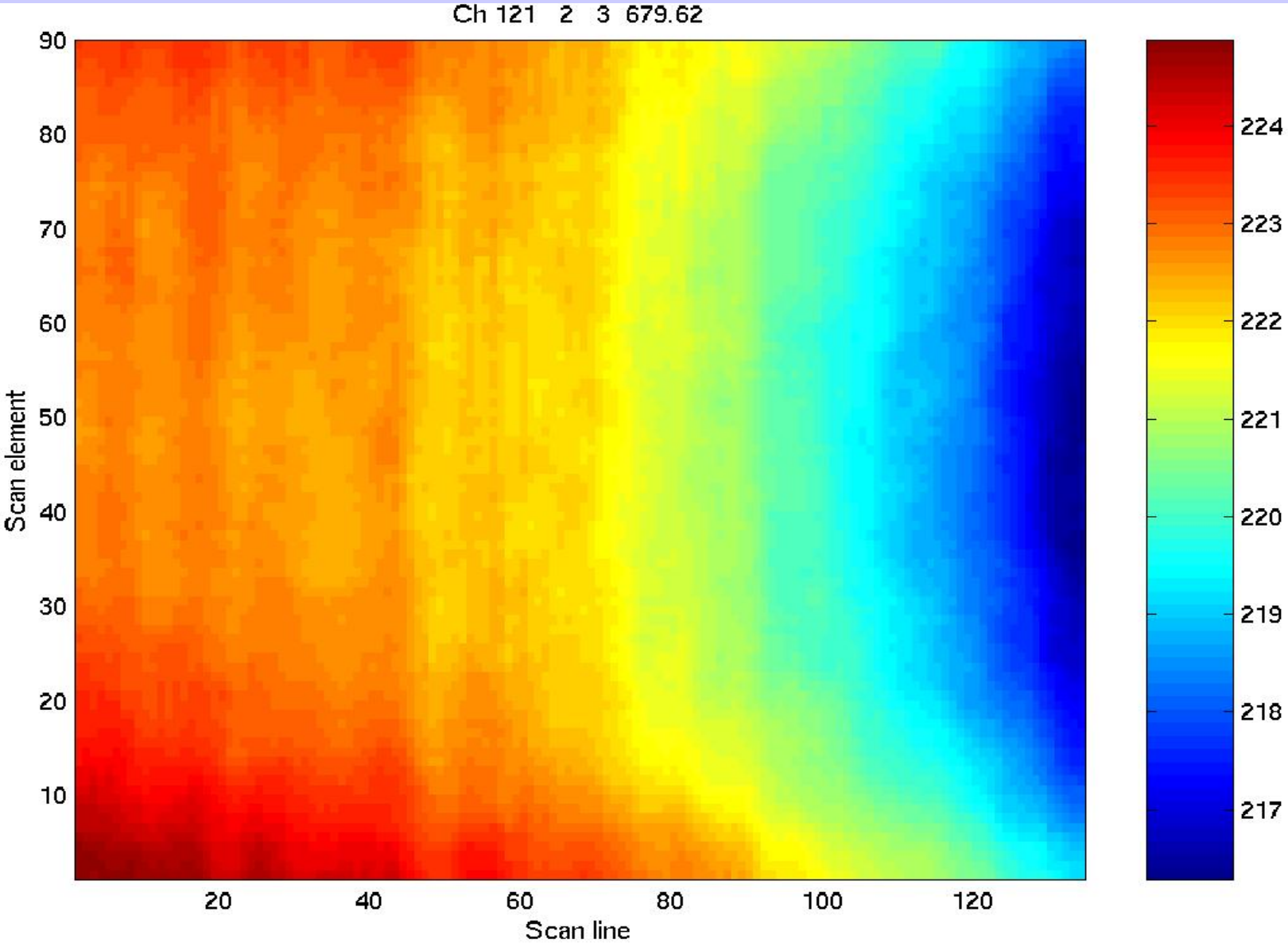

Spatial distribution of Ch 121 at 679.62 [1/cm] measurements [K]

original - filtered

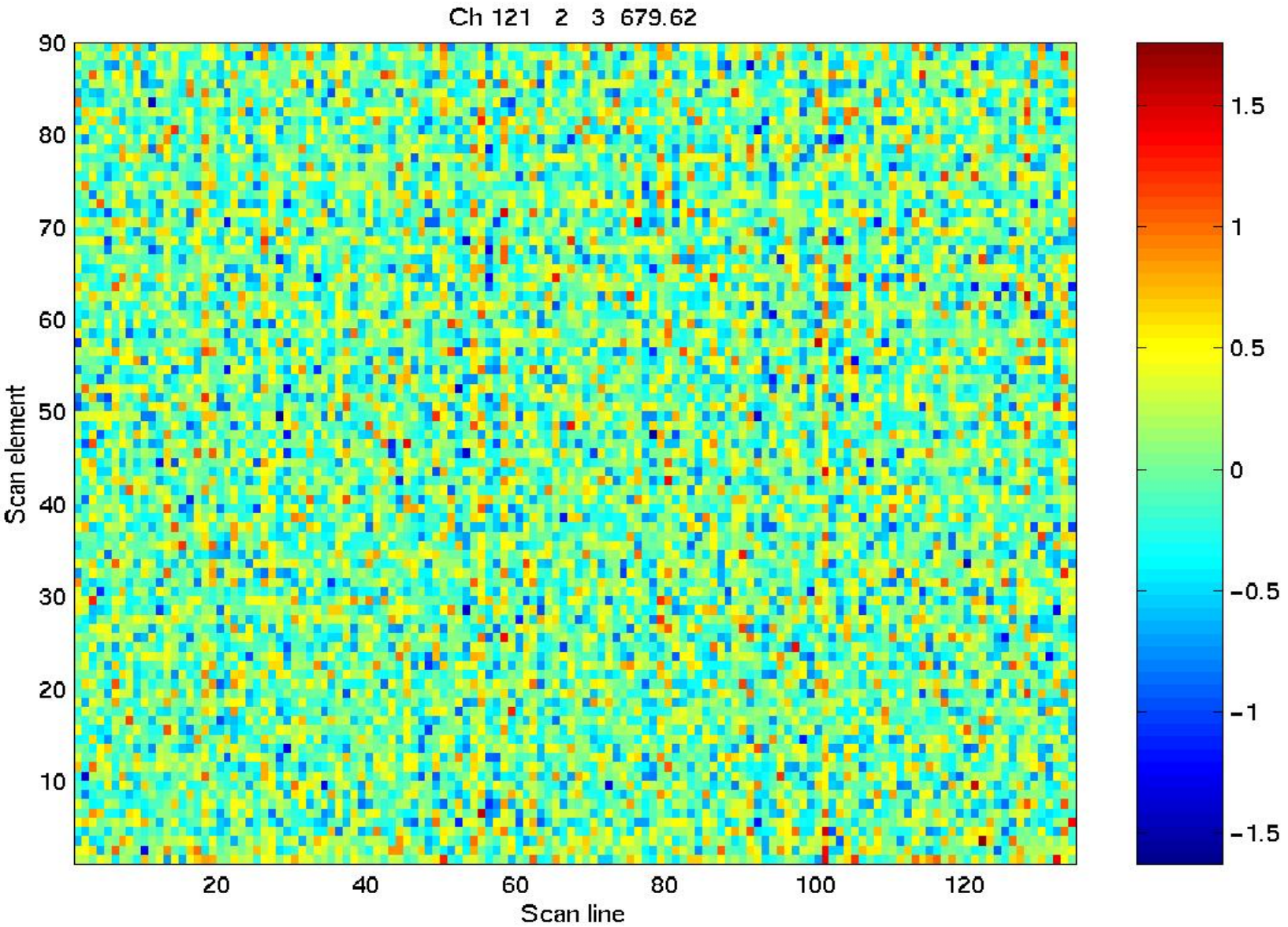

Spatial distribution of Ch 1789 at 1560.24 [1/cm] measurements [K]

original

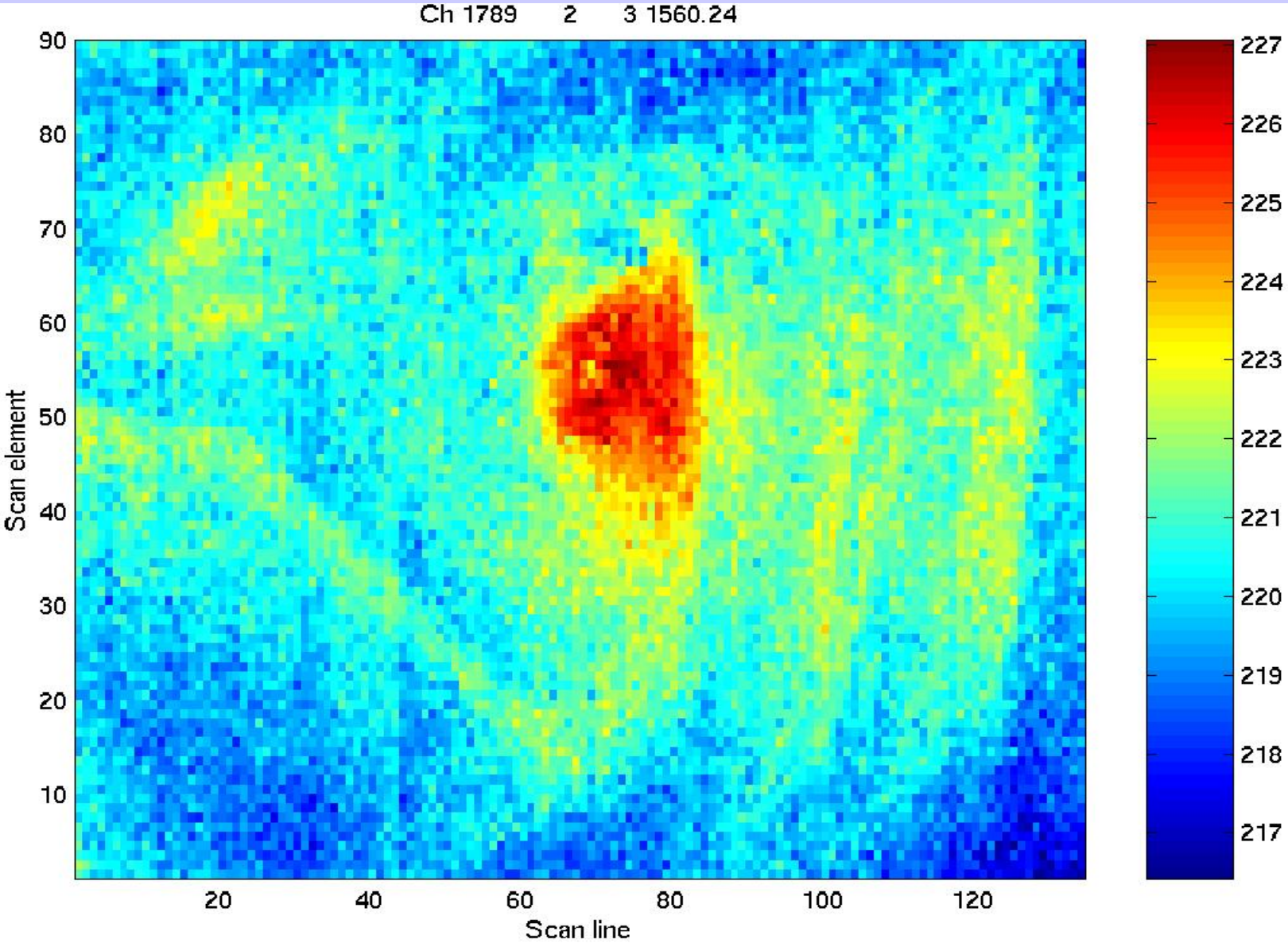

Spatial distribution of Ch 1789 at 1560.24 [1/cm] measurements [K] filtered

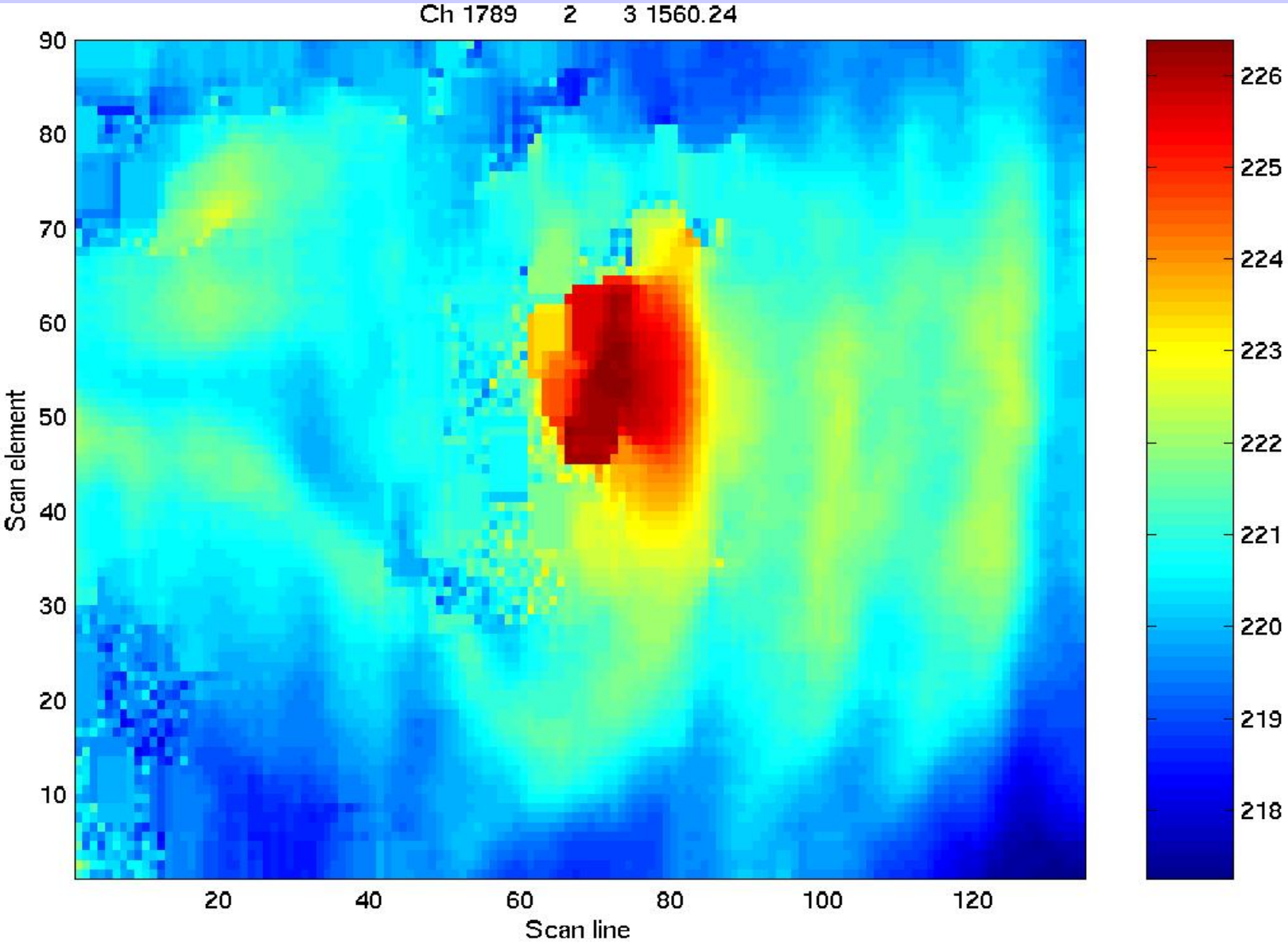

Spatial distribution of Ch 1789 at 1560.24 [1/cm] measurements [K]

original - filtered

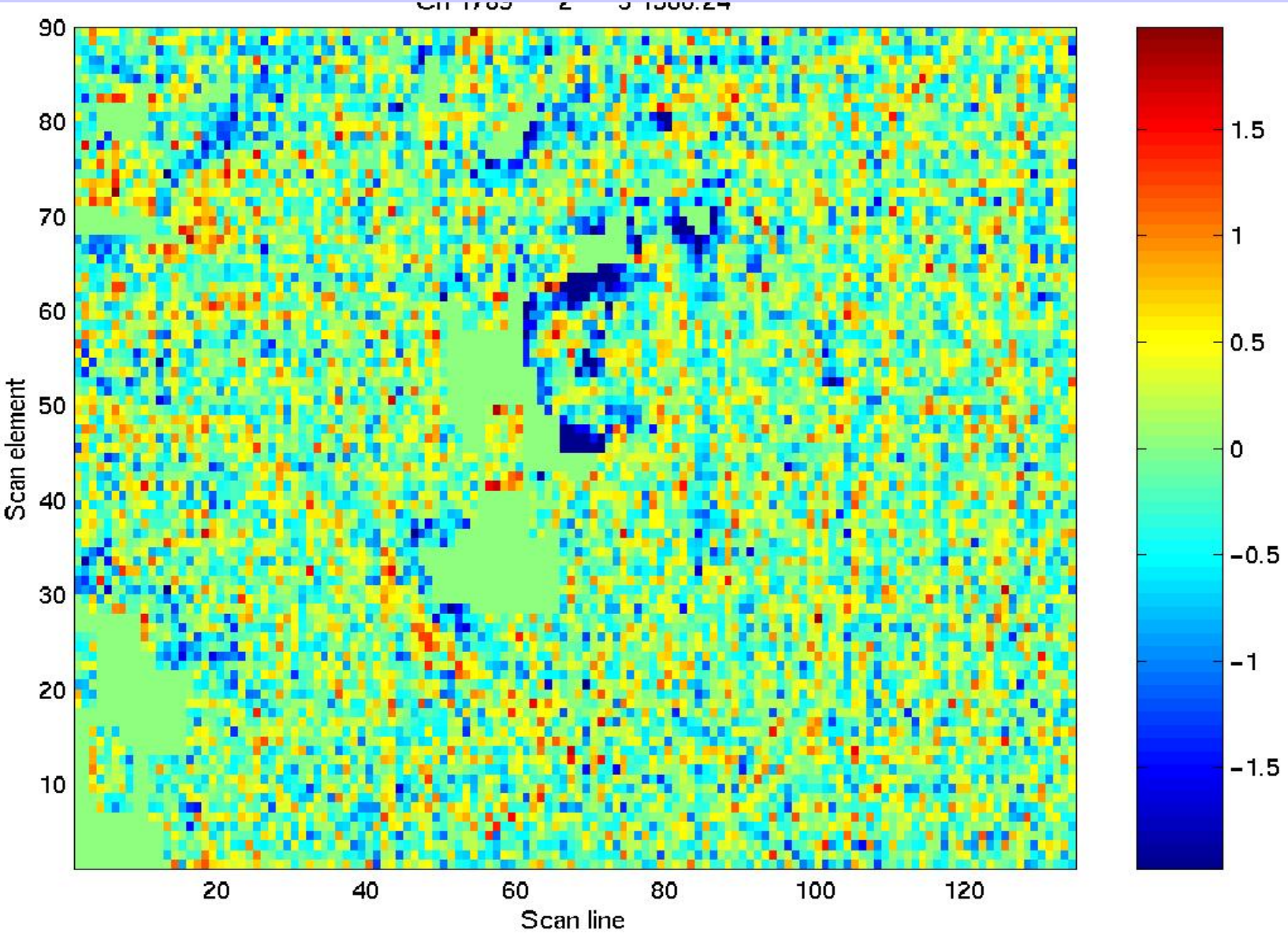

Spatial distribution of Ch 217 at 711.58 [1/cm] measurements [K]: original

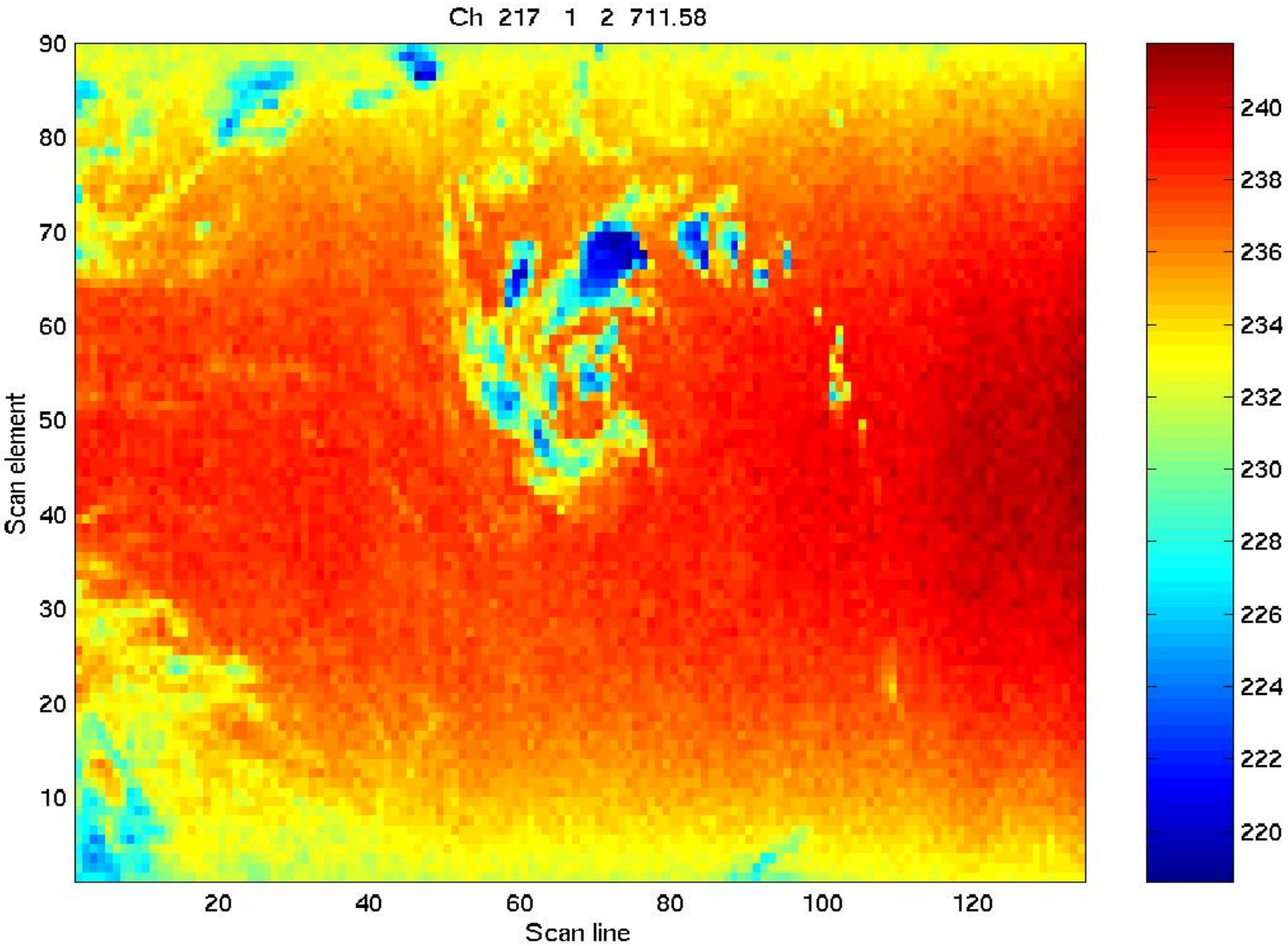

Spatial distribution of Ch 217 at 711.58 [1/cm] measurements [K]: filtered

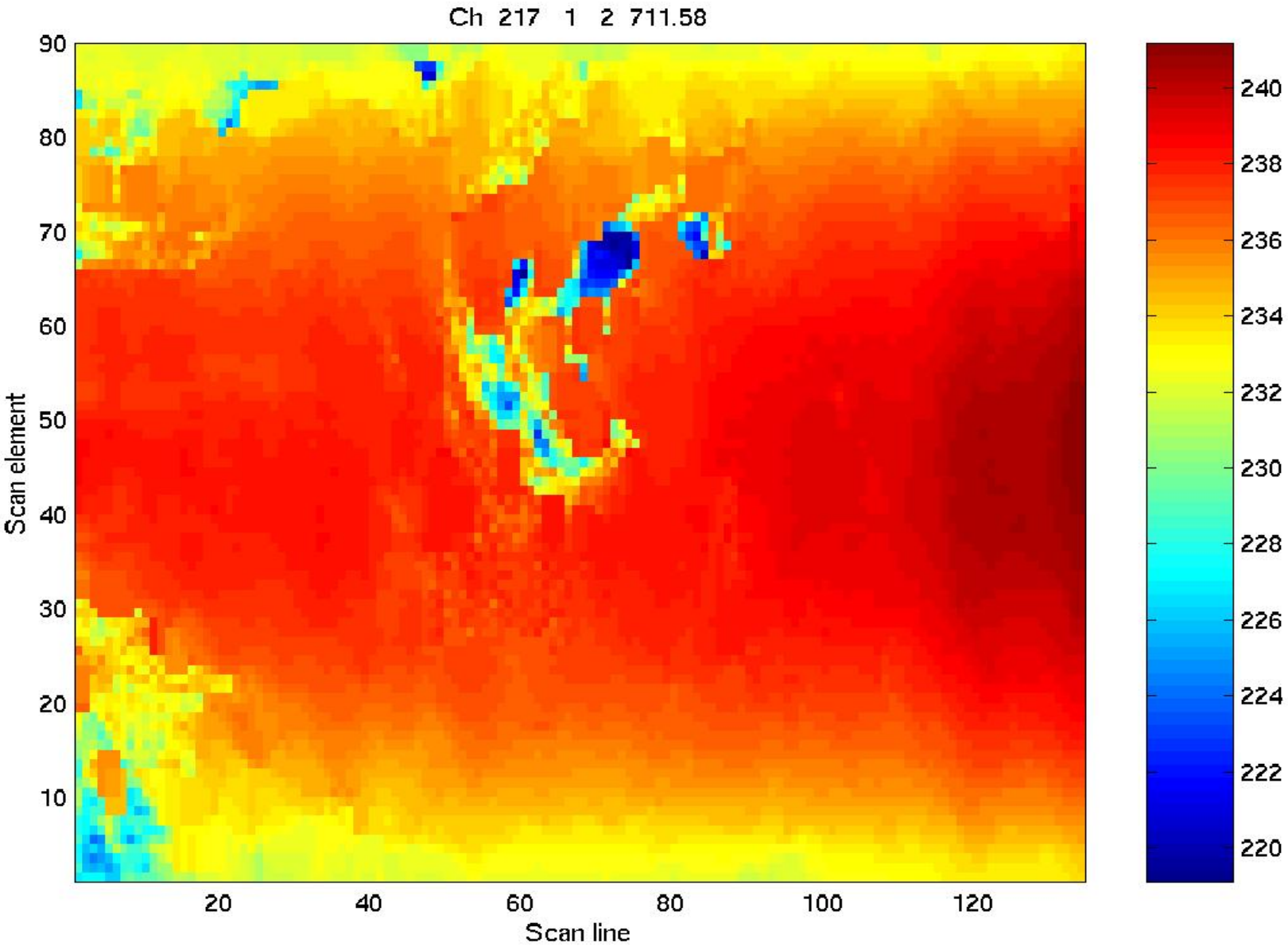

Spatial distribution of Ch 217 at 711.58 [1/cm] measurements [K]: original - filtered

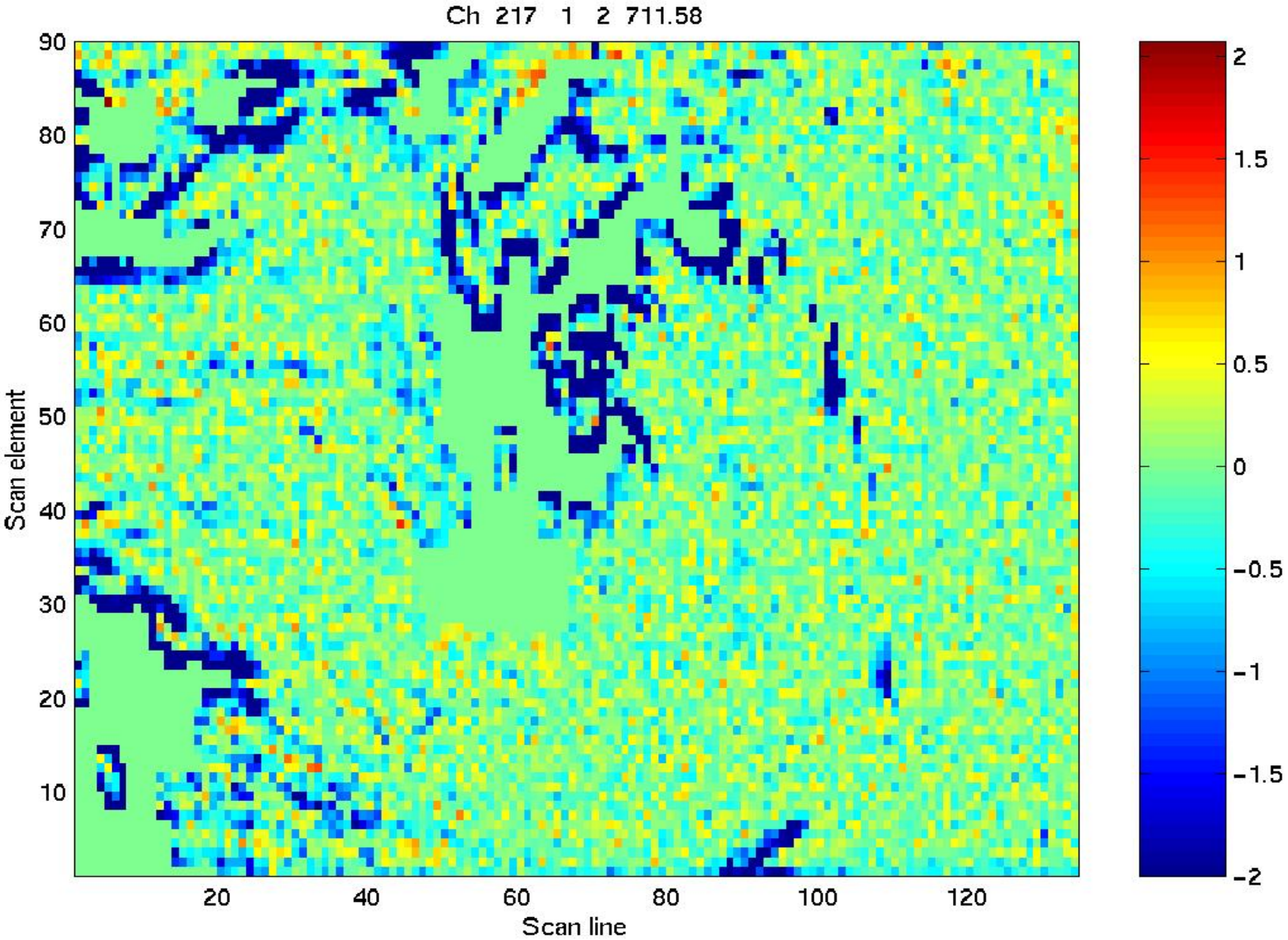

StDev of measurement error [K] after filtering derived from the spatial differential (GREEN)
StDev of measurement error [K] after filtering derived from bb measurement error [K] (PINK)
StDev of bb measurement error [K] (BLUE);

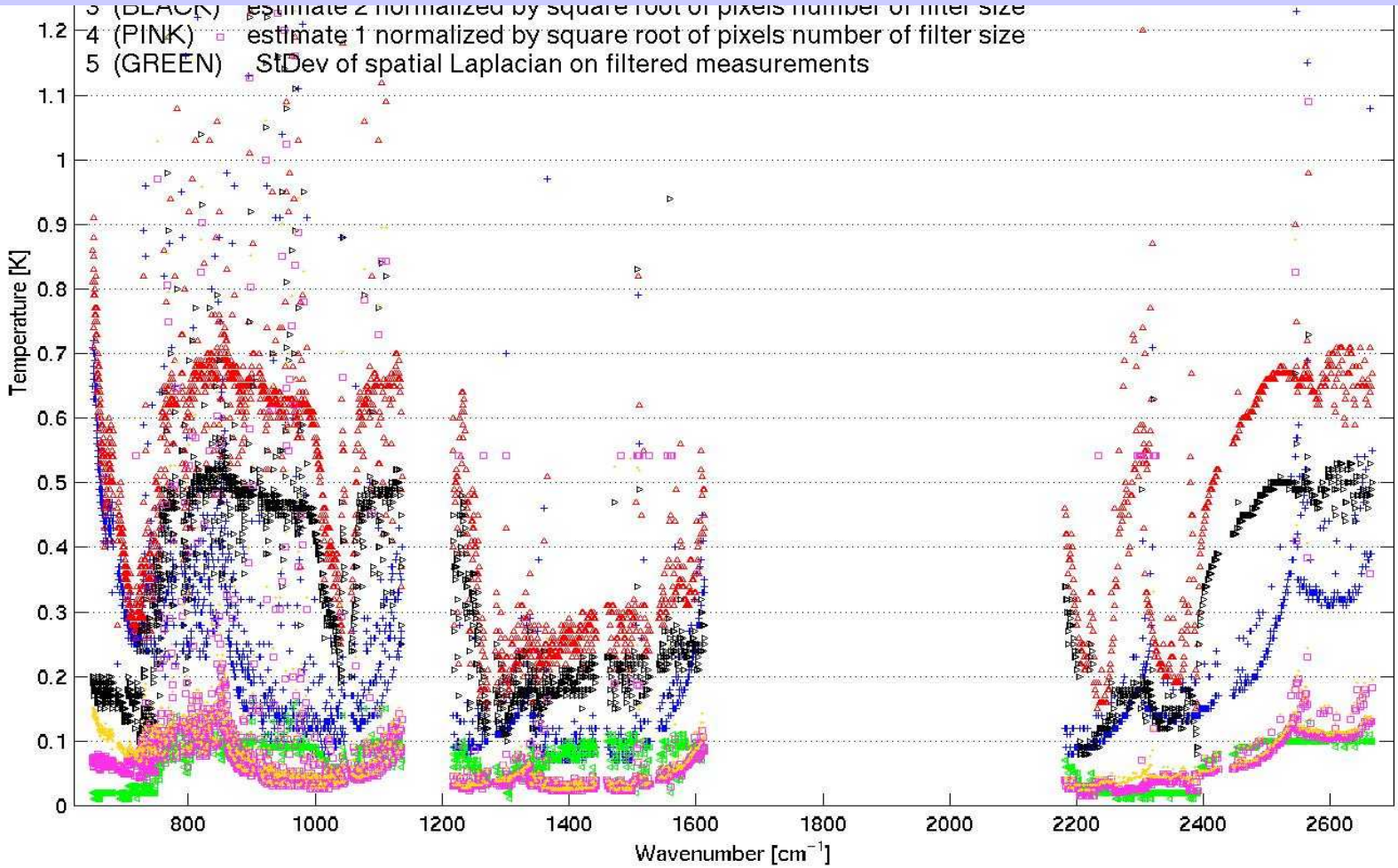

RTE for IR measurements

$$\tilde{\mathrm{J}}(\theta) = \varepsilon(\theta) B[\mathrm{T_s}]\tau_s^{\uparrow}(\theta) + \int_{\tau_s^{\uparrow}(\theta)}^{1} \mathrm{B}[\mathrm{T(p)}]\mathrm{d}\tau^{\uparrow}(\mathrm{p},\theta)$$

$$+ (1-\varepsilon(\theta))\tau_s^{\uparrow}(\theta) \int_{\tau_0^{\downarrow}(\vartheta^*)}^{1} \mathrm{B}[\mathrm{T(p)}]\mathrm{d}\tau^{\downarrow}(\mathrm{p},\vartheta^*) + \xi$$

Solution approach

Radiative transfer in earth-atmosphere system with a reflecting surface is modeled
Surface reflection is described by hemispherical directional effective emissivity for a effective angle of incidence

Solution parameters include emissivity spectrum, surface temperature, atmospheric moisture and temperature profiles.

Emissivity spectrum variation was parametrically defined (N=11)
Atmospheric moisture profile variation was parametrically defined (N=17)
Atmospheric temperature profile variation was parametrically defined (N=31)
Problem dimensionality N=60

Non-linear Fredholm equation of first kind is solved using method of least squares (regularized wrt atmospheric parameters) in coordinate descent on basis of a Gauss-Newton numerical schema.

Number of analyzed spectral channels around 2100

Iterative algorithm of solution

$$\varepsilon^{(0)} = 0.92 \quad , \quad T_s^{(0)} = \bar{T}_s \quad , \quad T(p)^{(0)} = \bar{T}(p) \quad , \quad W(p)^{(0)} = \bar{W}(p)$$

$$\left.\begin{aligned} &\varepsilon^{(n+1)} = \arg\min_{\varepsilon} \left\| \tilde{J} - J[\varepsilon, T_s^{(n)}, T(p)^{(n)}, W(p)^{(n)}] \right\|^2_{D^{-1}} \\ &\varepsilon \in [\ 0.6\ ,\ 0.985] \end{aligned}\right\}_{\Omega_S} \qquad (I)$$

$$\left.\begin{aligned} &x_s^{(n+1)} = \arg\min_{x_s} \left\| \tilde{J} - J[\varepsilon^{(n+1)}, T_s^{(n)} + x_s, T(p)^{(n)}, W(p)^{(n)}] \right\|^2_{D^{-1}} \\ &T_s^{(n+1)} = T_s^{(n)} + x_s^{(n+1)} \end{aligned}\right\}_{\Omega_S} \qquad (II)$$

$$\left.\begin{aligned} &\begin{bmatrix} x(p)^{(n+1)} \\ w(p)^{(n+1)} \end{bmatrix} = \arg\min_{\substack{x(p) \\ w(p)}} \left\{ \begin{aligned} &\left\| \tilde{J} - J[\varepsilon^{(n+1)}, T_s^{(n+1)}, T(p)^{(n)} + x(p), W(p)^{(n)} + w(p)] \right\|^2_{S^{-1}} \\ &+ \left\| T(p)^{(n)} + x(p) - \bar{T}(p) \right\|^2_{R_x^{-1}} + \left\| W(p)^{(n)} + w(p) - \bar{W}(p) \right\|^2_{R_w^{-1}} \end{aligned} \right\} \\ &T(p)^{(n+1)} = T(p)^{(n)} + x(p)^{(n+1)} \quad , \quad W(p)^{(n+1)} = W(p)^{(n)} + w(p)^{(n+1)} \end{aligned}\right\}_{\Omega_T, \Omega_W} \qquad (III)$$

$$n := n+1 \quad for \quad \left\| \tilde{J} - J[\varepsilon^{(n+1)}, T_s^{(n+1)}, T(p)^{(n+1)}, W(p)^{(n+1)} \right\|^2_{S^{-1}} > Sp(D^{-1}S)$$

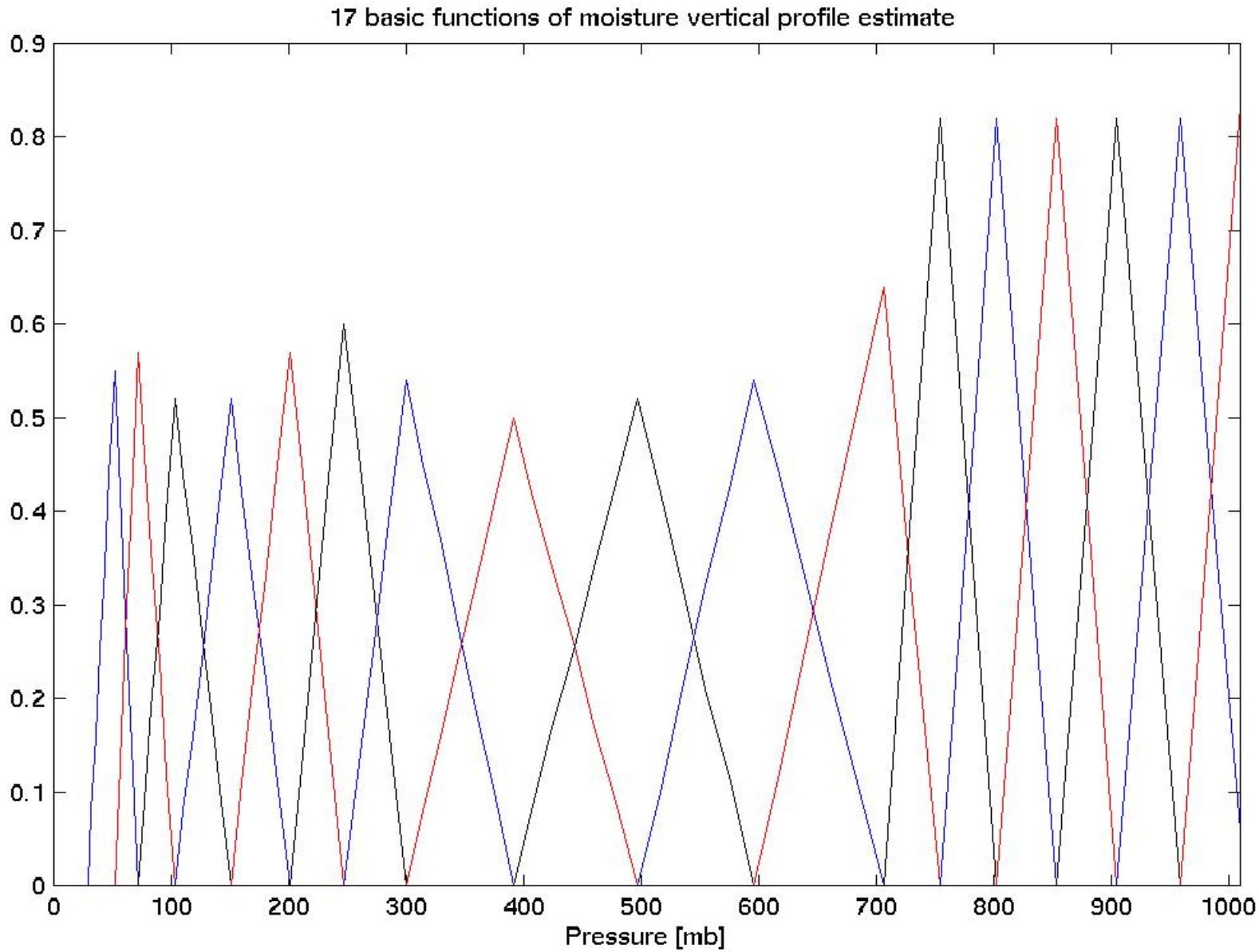
17 basic functions of moisture vertical profile estimate
0.9
0.8
0.7
0.6
0.5
0.4
0.3
0.2
0.1
0
0
100
200
300
400
500
600
700
800
900
1000
Pressure [mb]

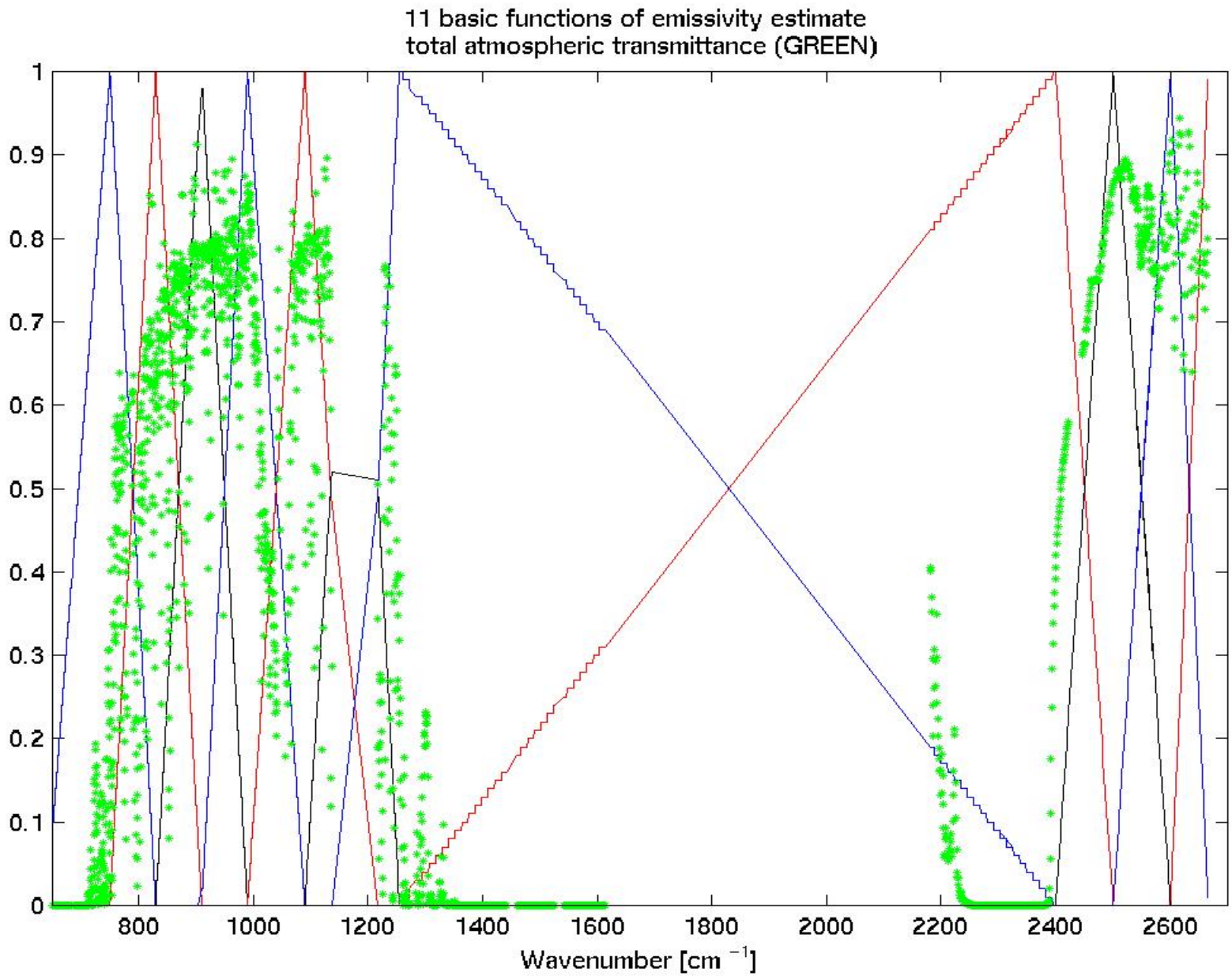
11 basic functions of emissivity estimate
total atmospheric transmittance (GREEN)
1
0.9
0.8
0.7
0.6
0.5
0.4
0.3
0.2
0.1
0
800
1000
1200
1400
1600
1800
2000
2200
2400
2600
Wavenumber [cm $^{-1}$]

Radiance response [%] to emissivity variation (.94 - .96)

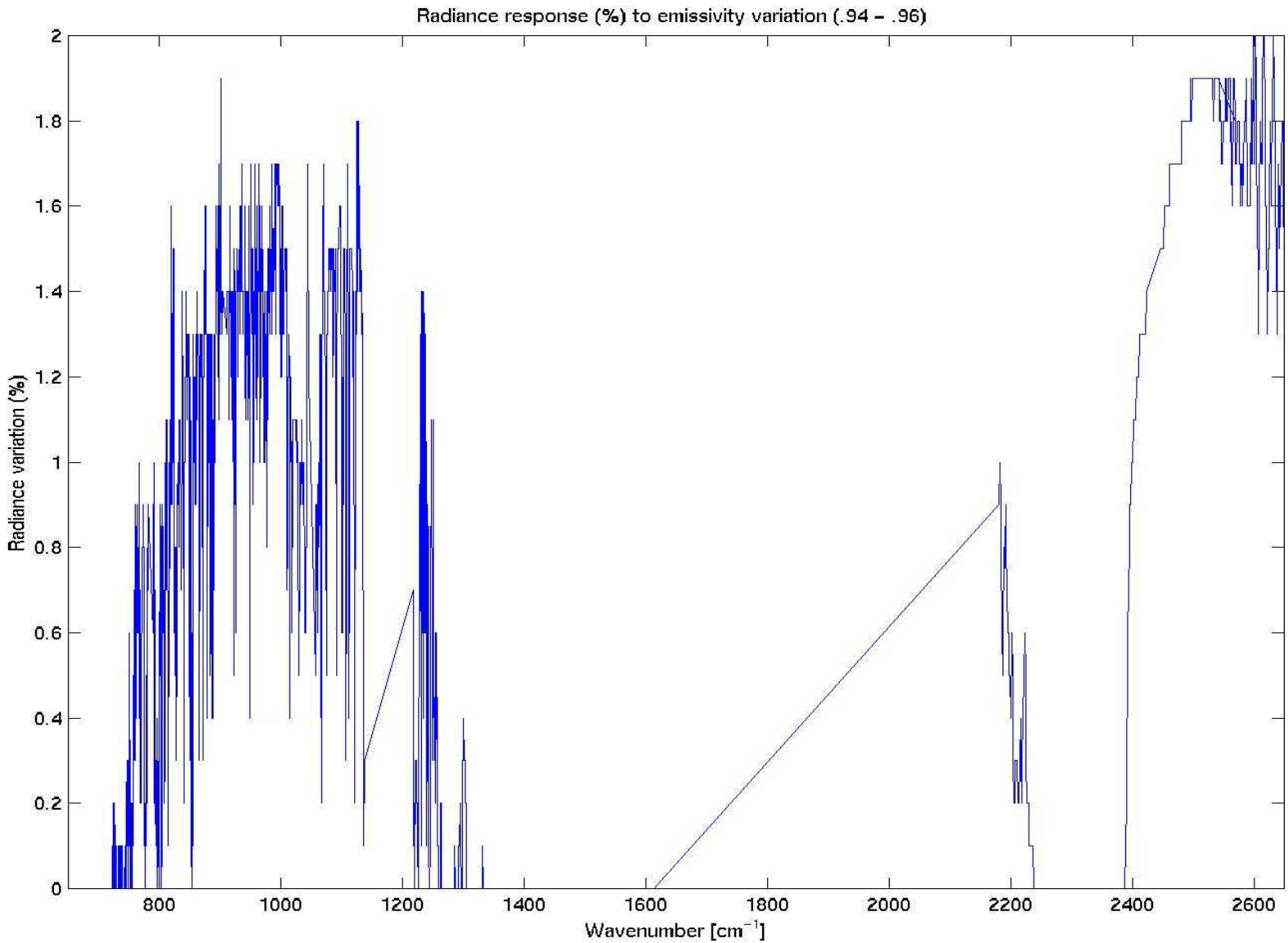

Example of spatial (latitudinal) crossection of emissivity estimates over North Africa (Sahara)

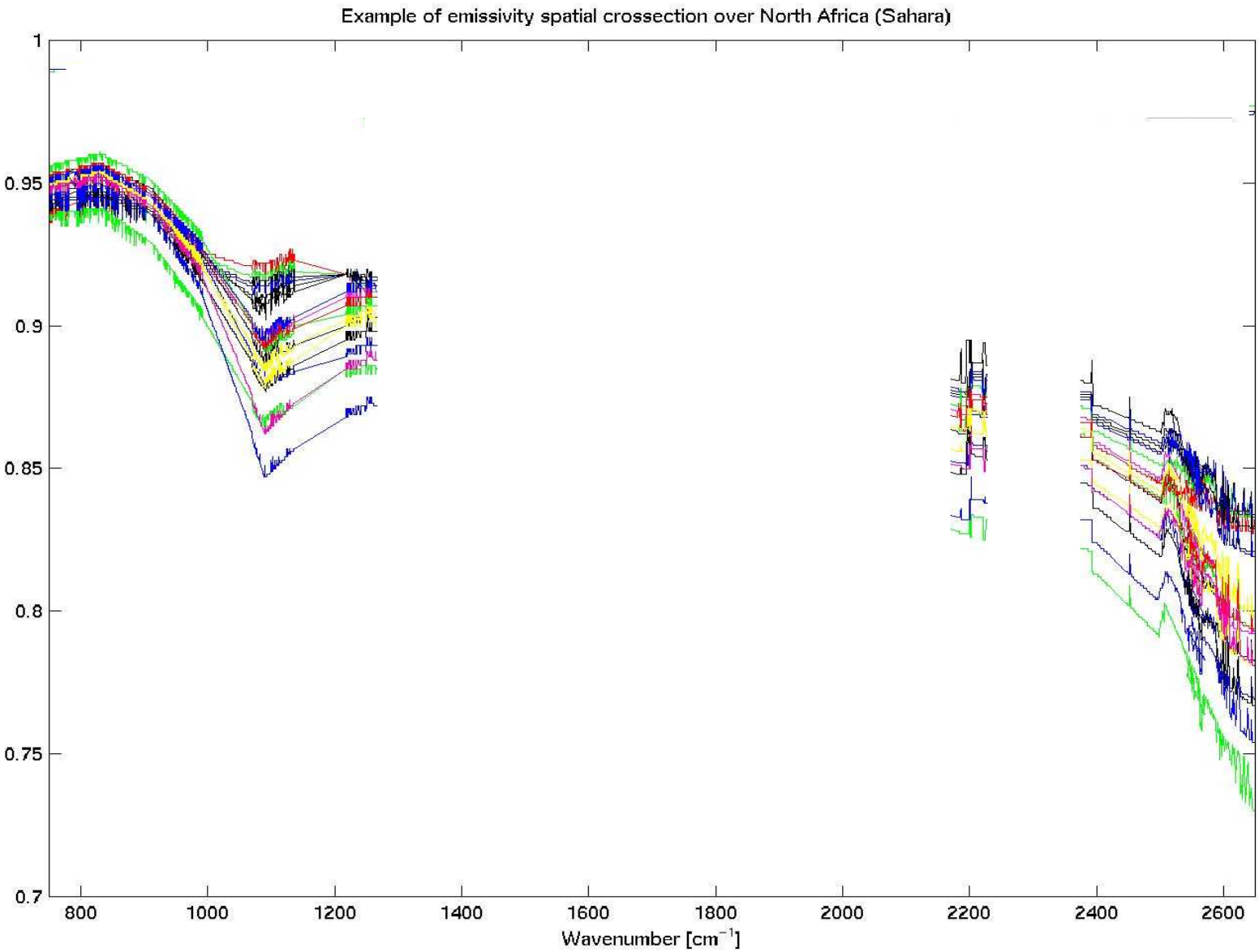

Laboratory measurements of surface reflection: SAND

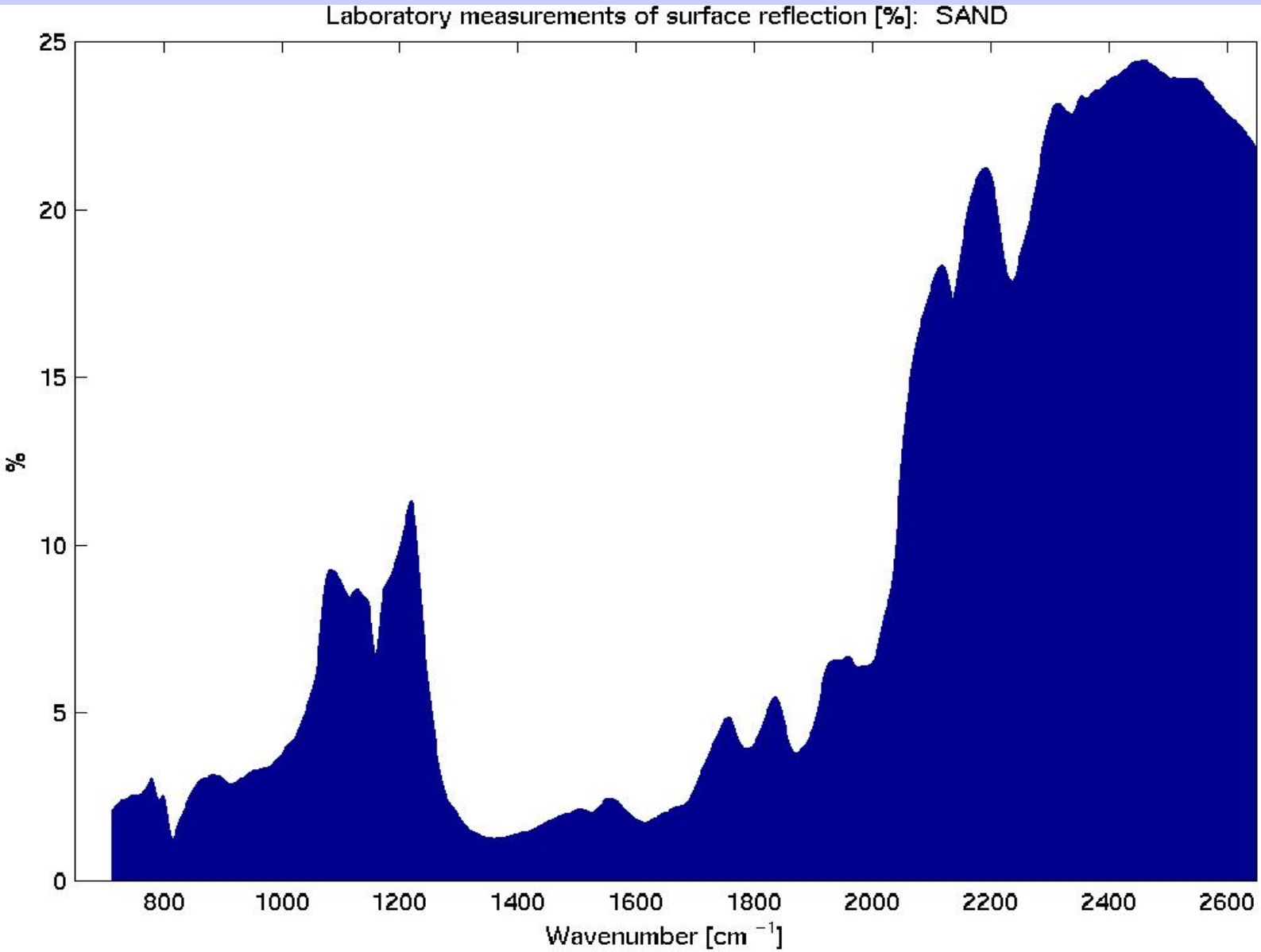

Laboratory measurements of surface reflection: BASALT

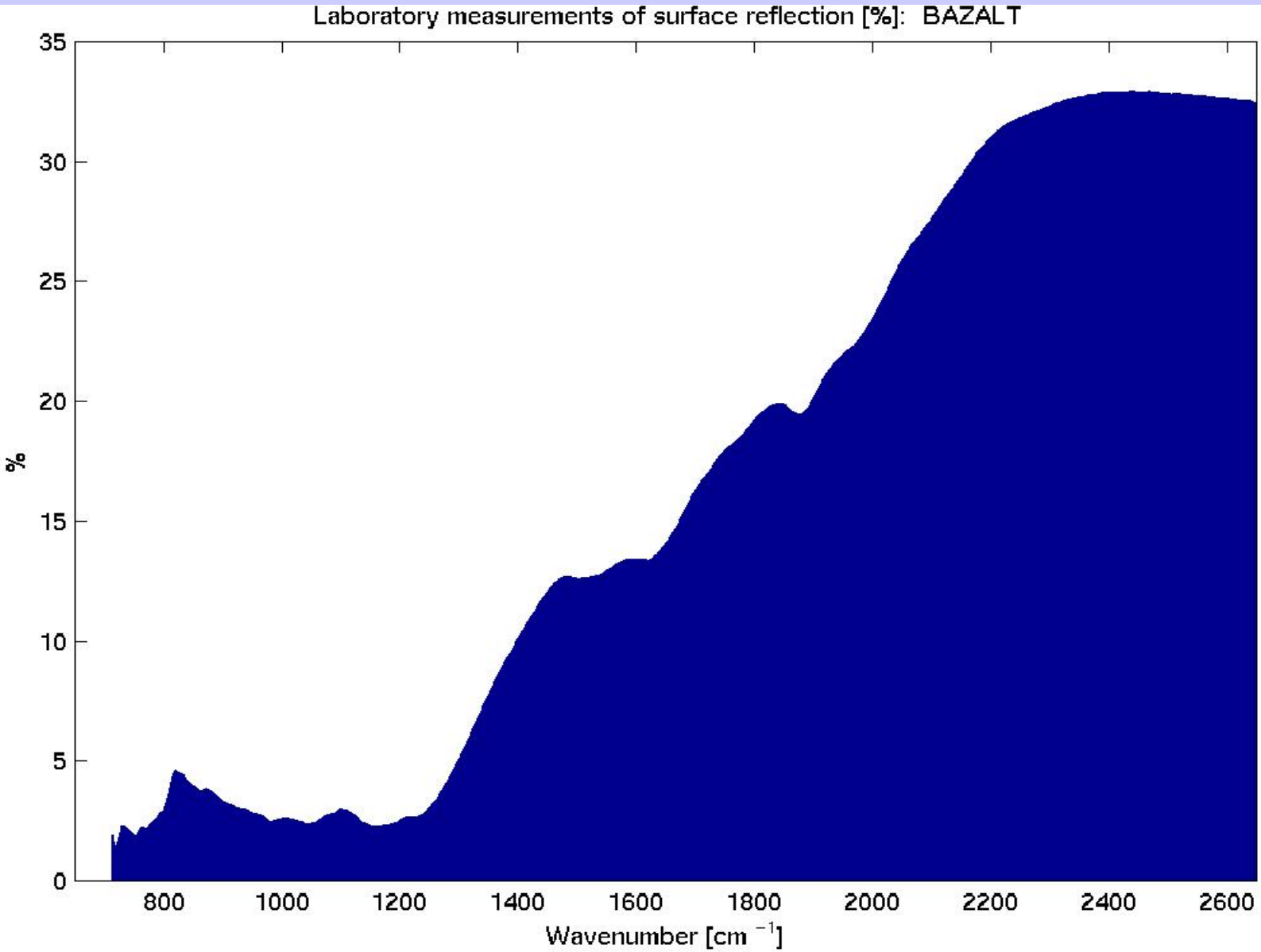

Laboratory measurements of surface reflection: GRANITE

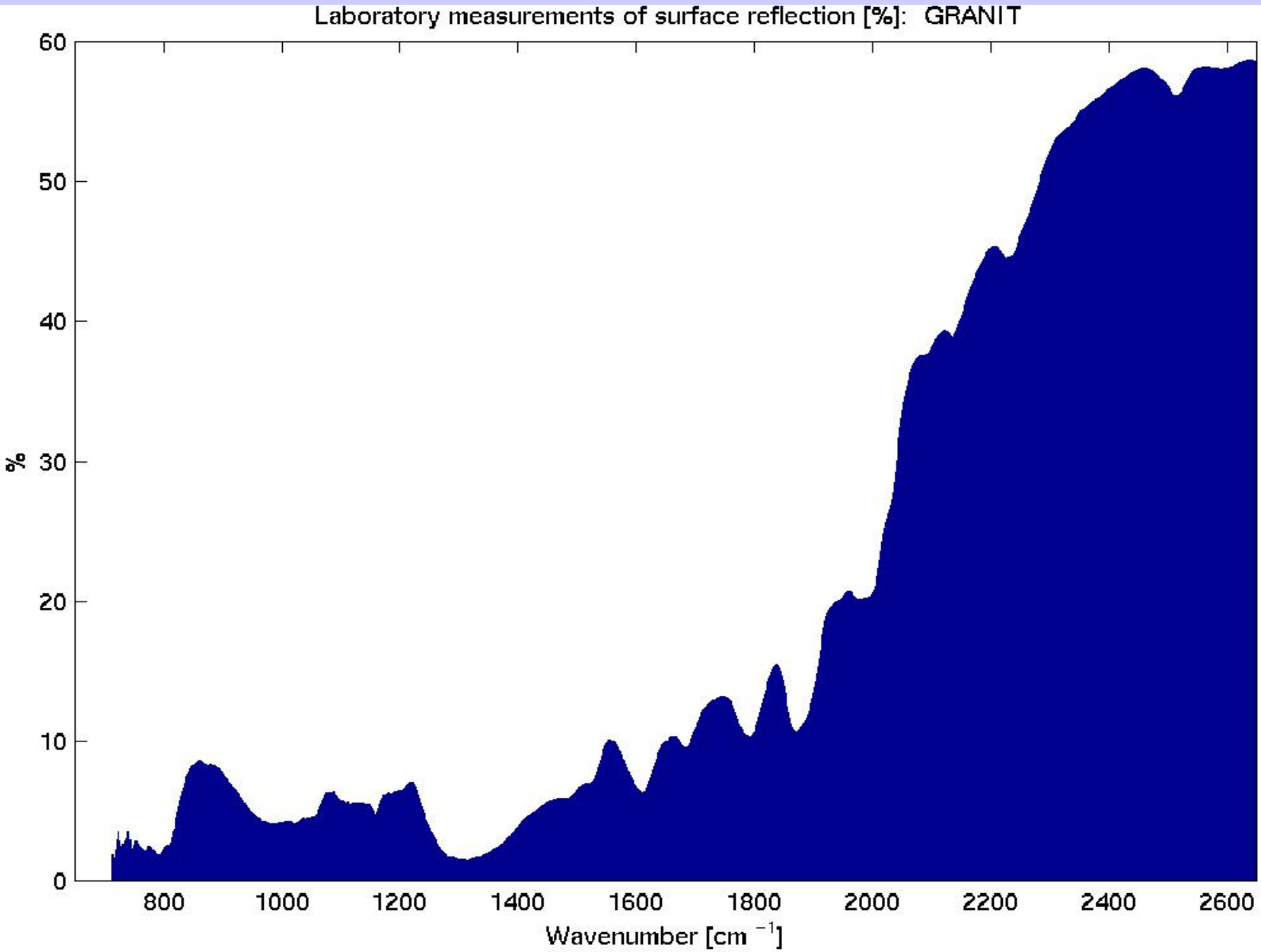

Laboratory measurements of surface reflection: SOIL

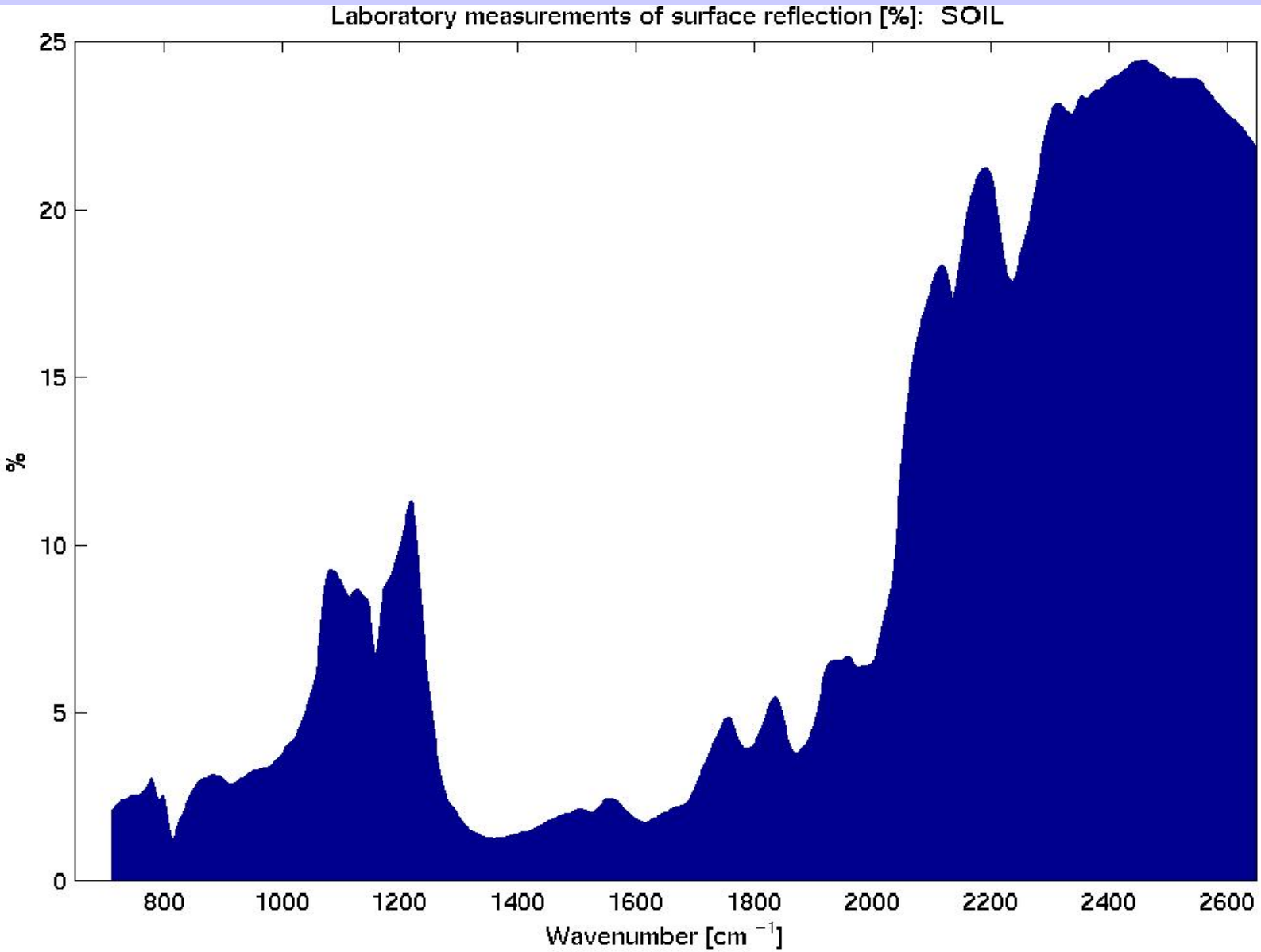

Spatial distribution of emissivity estimate

Ch 770 at 911.23 [1/cm]

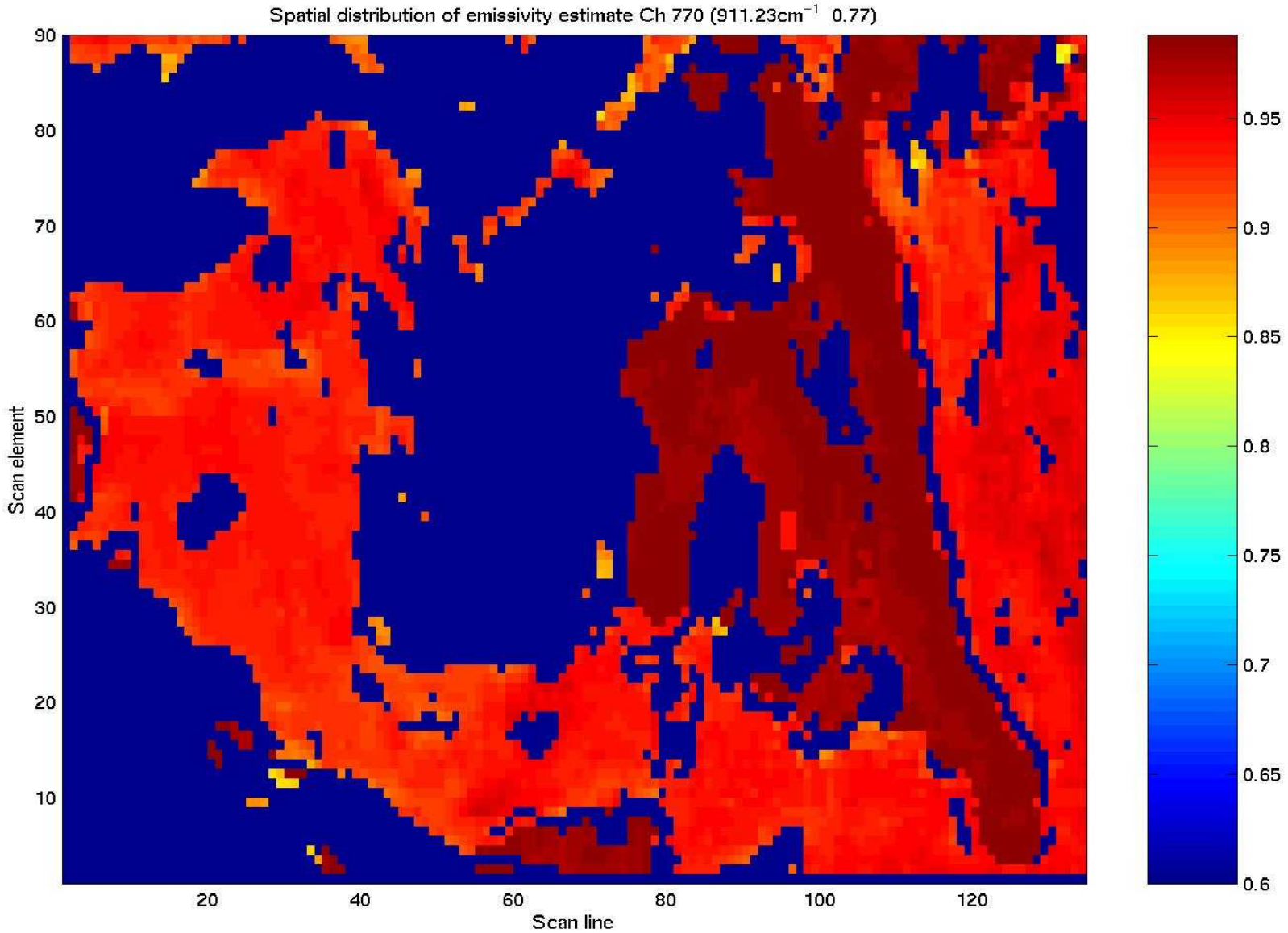

Spatial distribution of emissivity estimate

Ch 977 at 990.34 [1/cm]

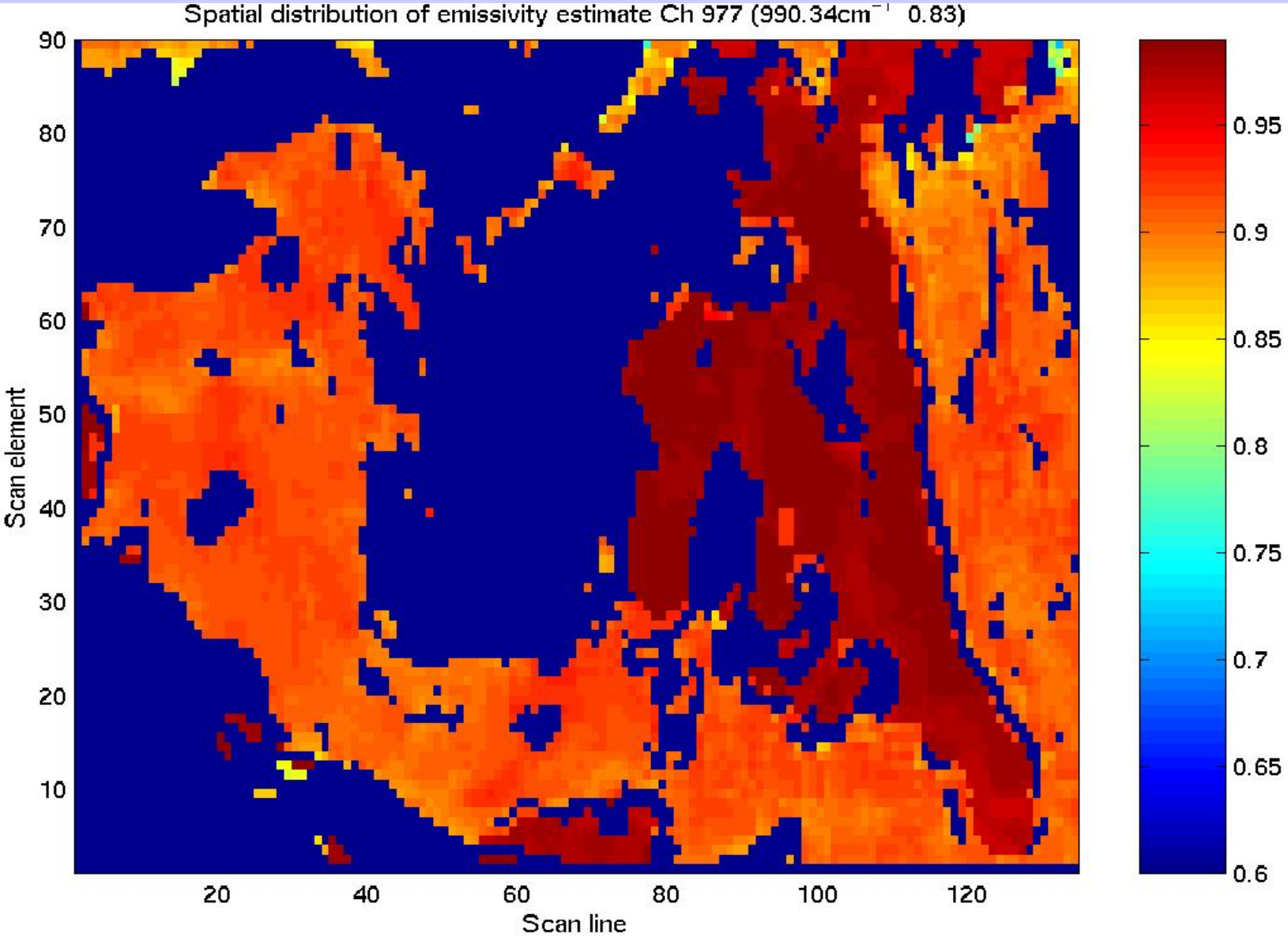

Spatial distribution of emissivity estimate

Ch 1246 at 1127.99 [1/cm]

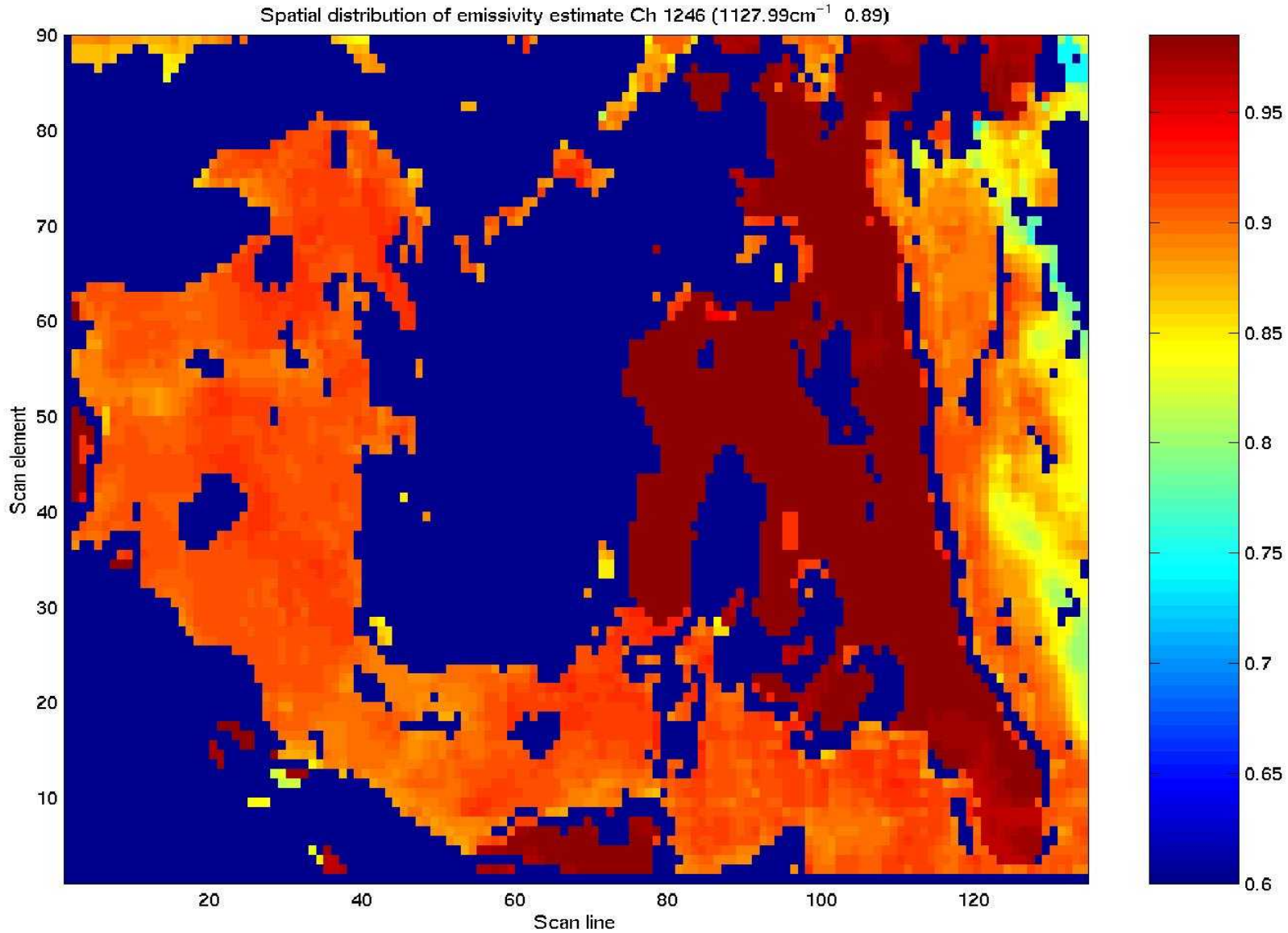

Spatial distribution of emissivity estimate

Ch 1297 at 1234.45 [1/cm]

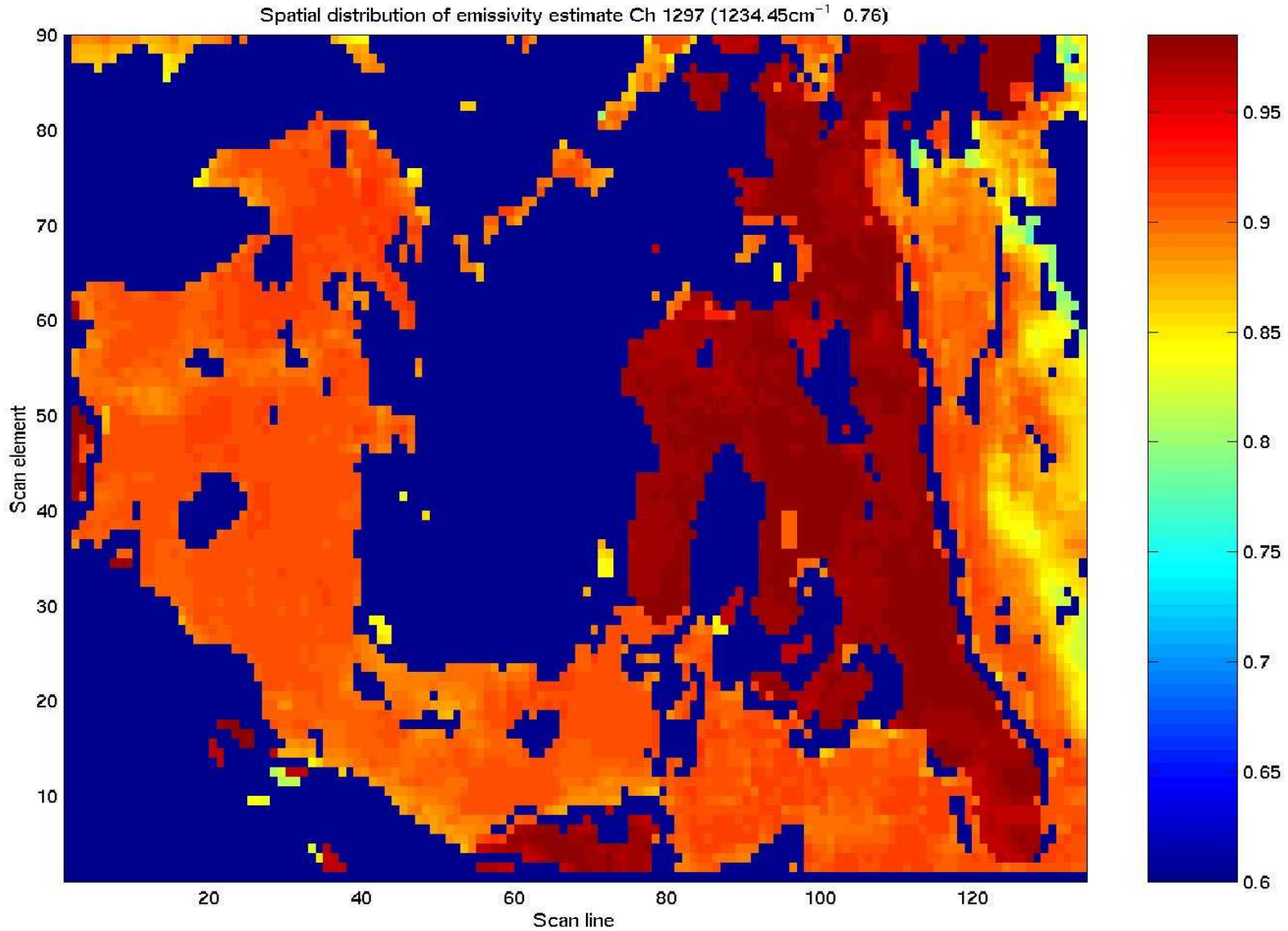

Spatial distribution of emissivity estimate

Ch 2197 at 2500.6 [1/cm]

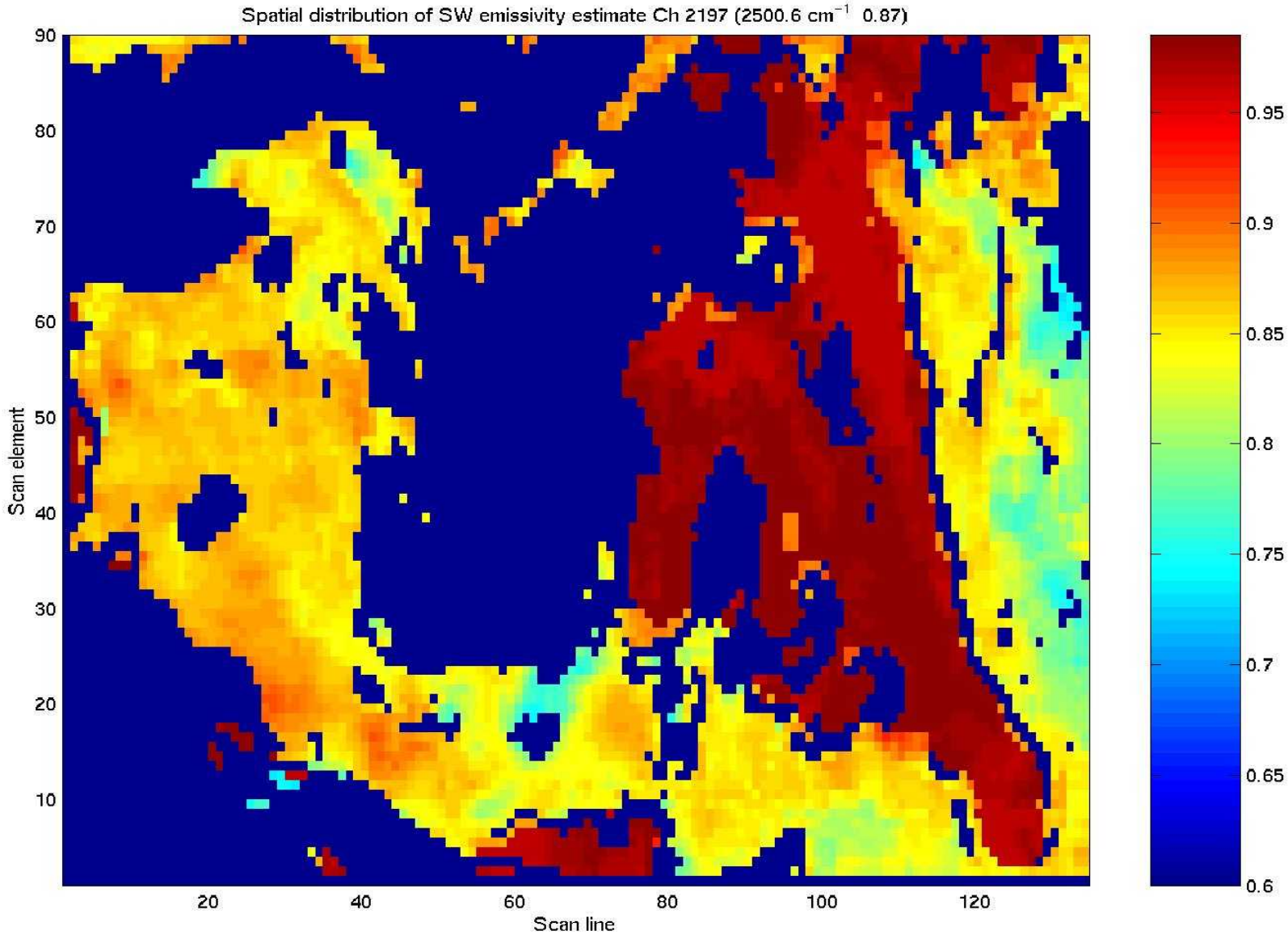

Spatial distribution of emissivity estimate

Ch 2333 at 2616.38 [1/cm]

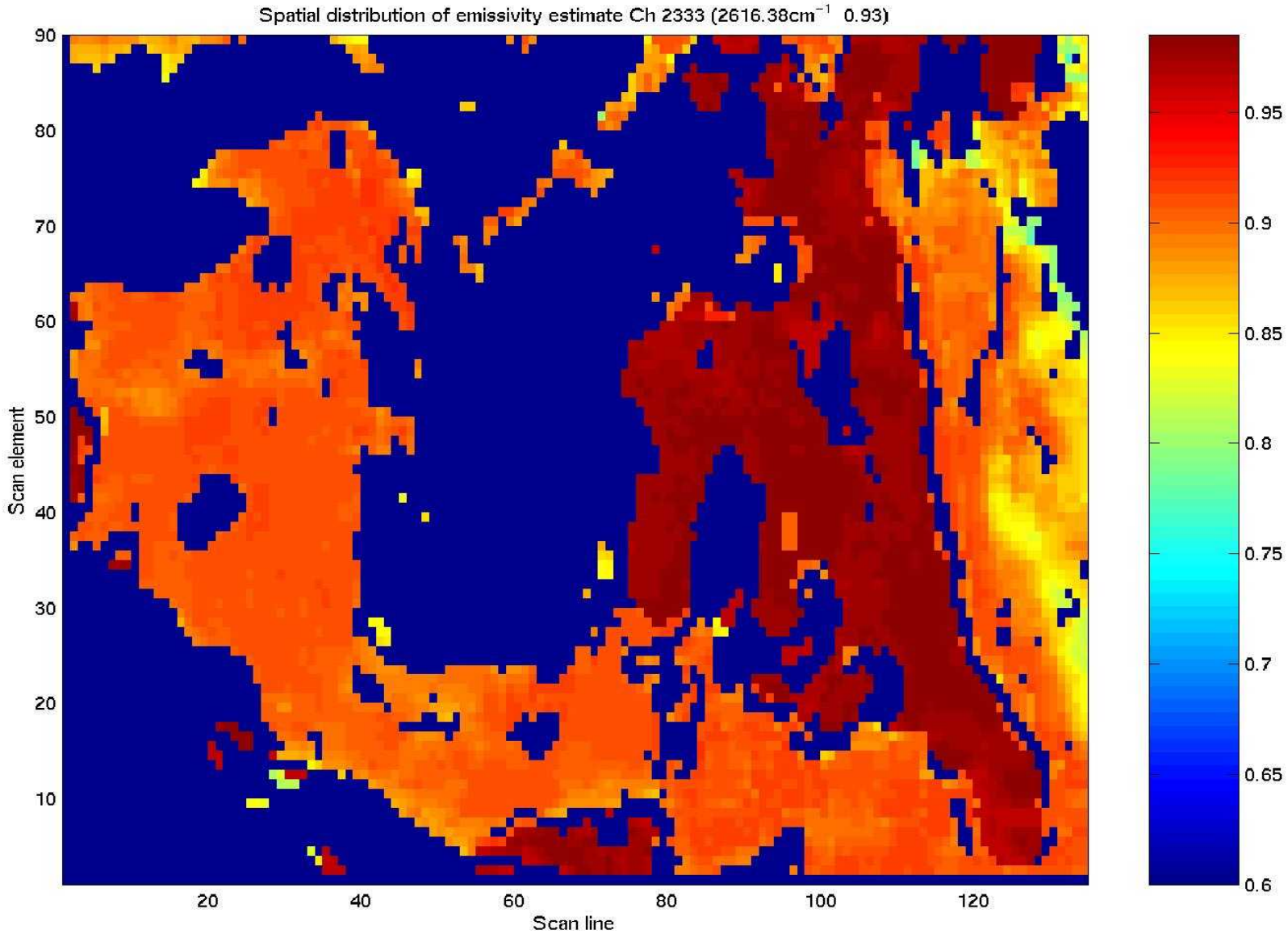

Spatial distribution of surface temperature estimate [K]

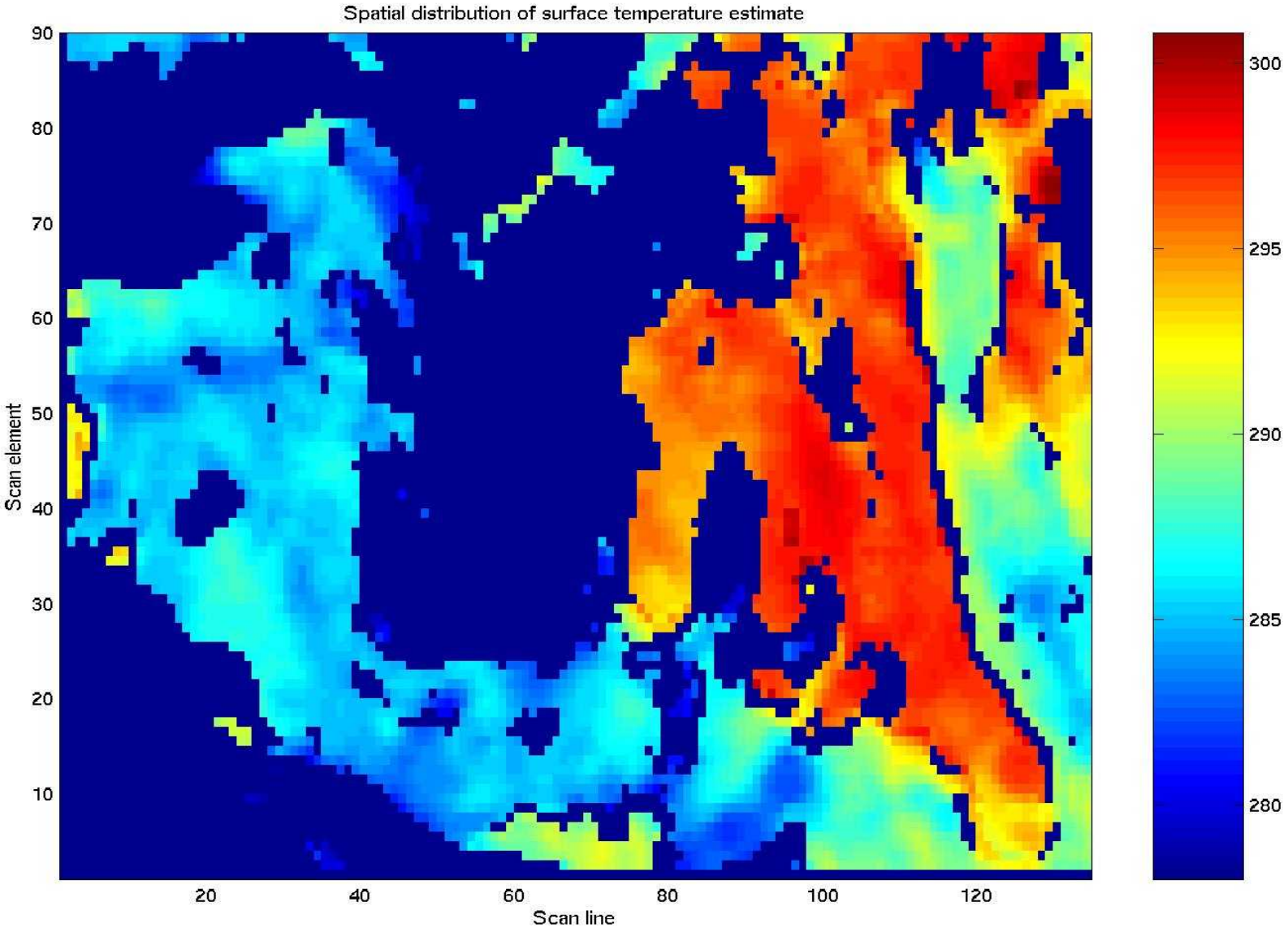

Spatial distribution of surface temperature first guess [K]

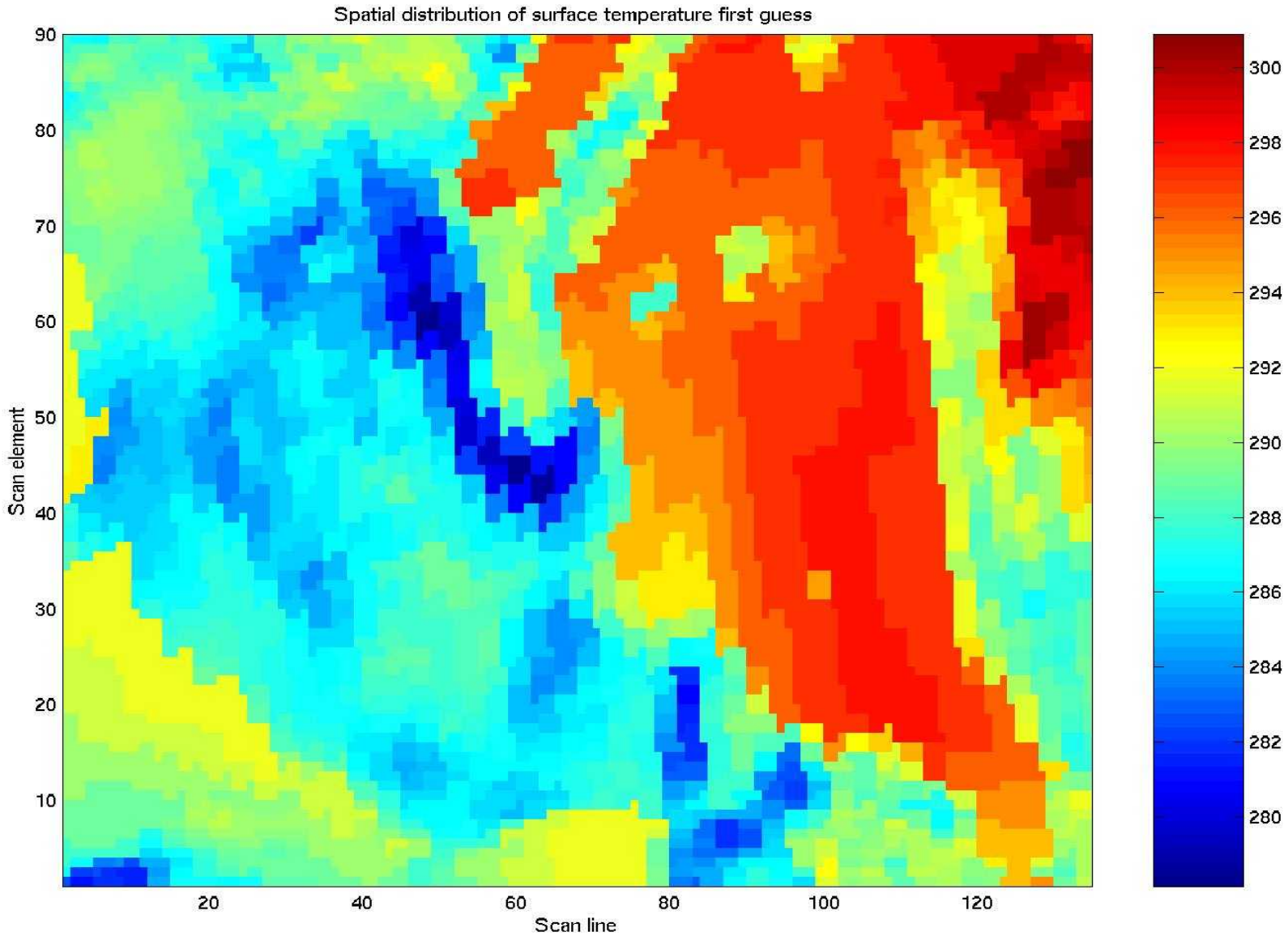

Spatial distribution of moisture [%] at 300mb estimate & first guess

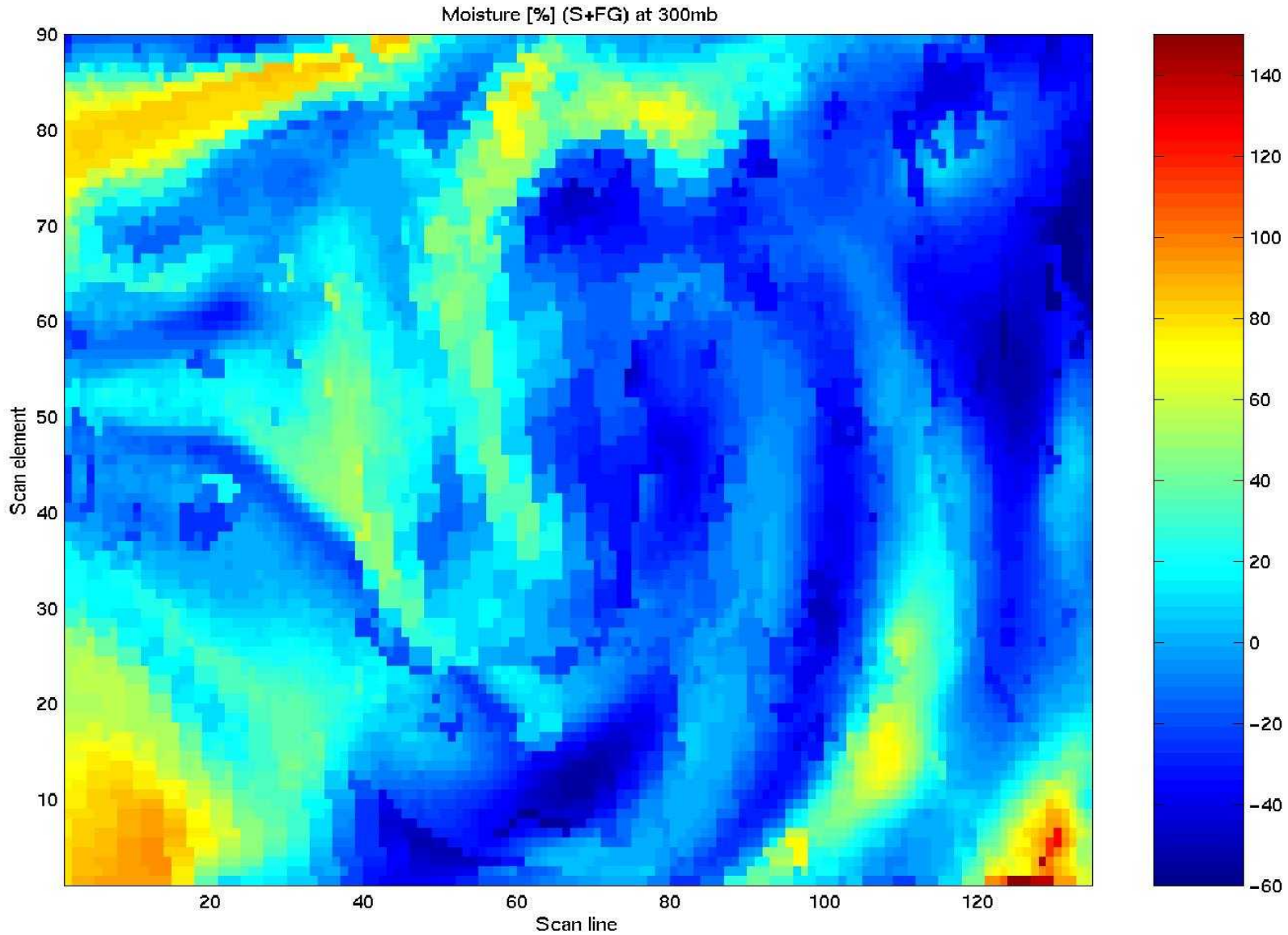

Spatial distribution of moisture [%] at 300mb first guess

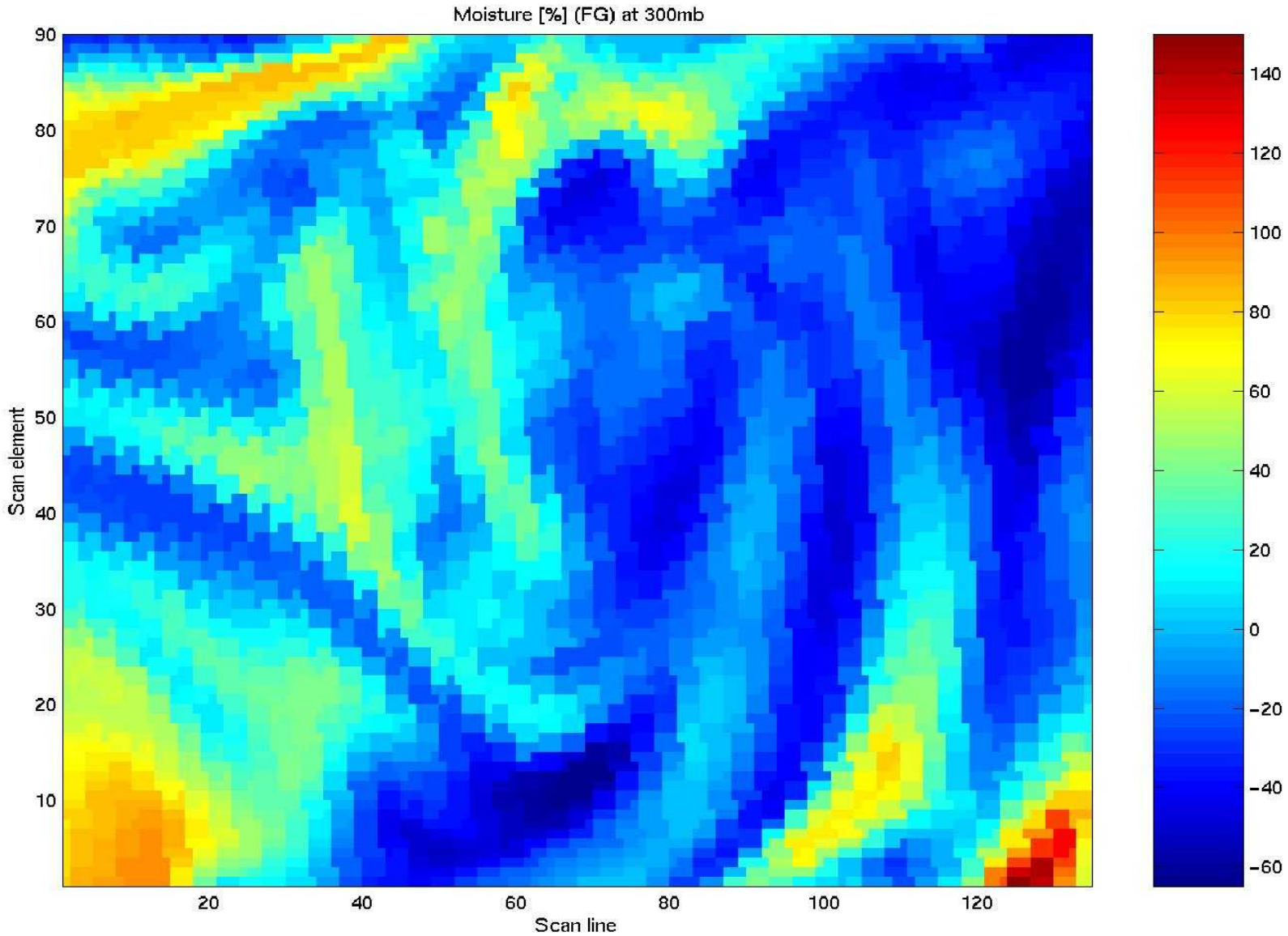

Spatial distribution of moisture [%] at 500mb estimate & first guess

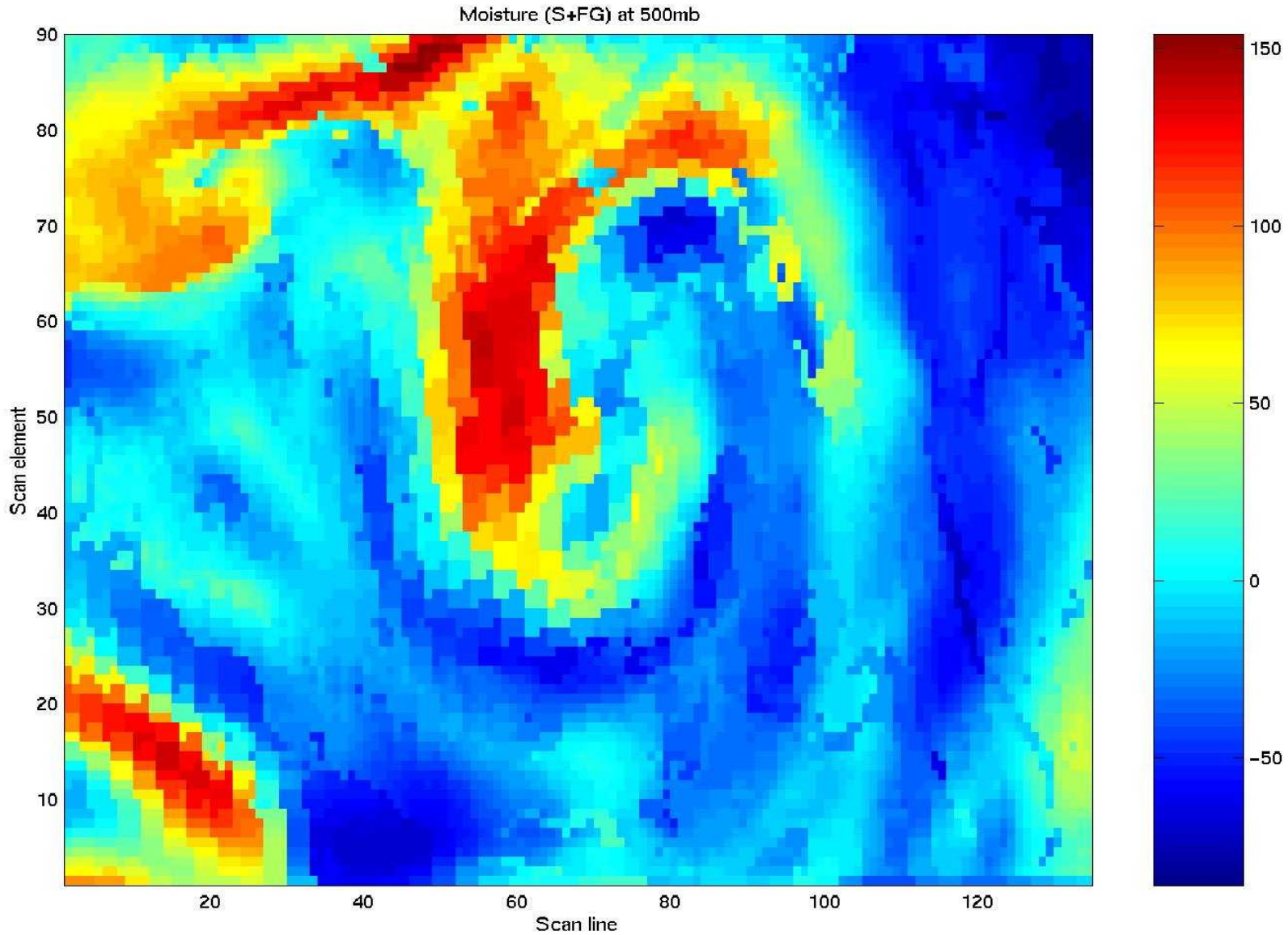

Spatial distribution of moisture [%] at 500mb first guess

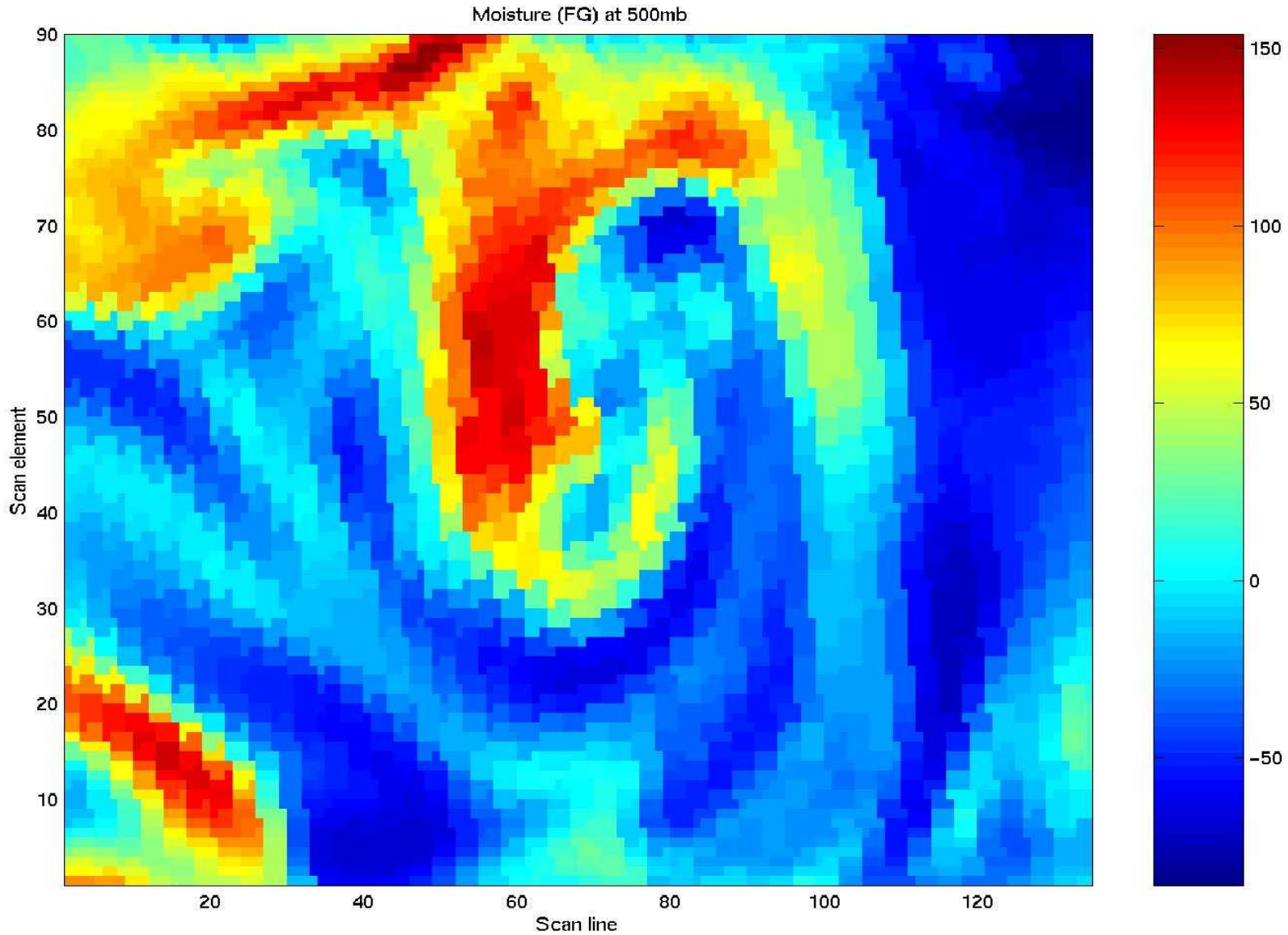

Statistics of residuals [K] (a) - over Land , (b) - over Ocean

Average - Black, StDev - Red

a

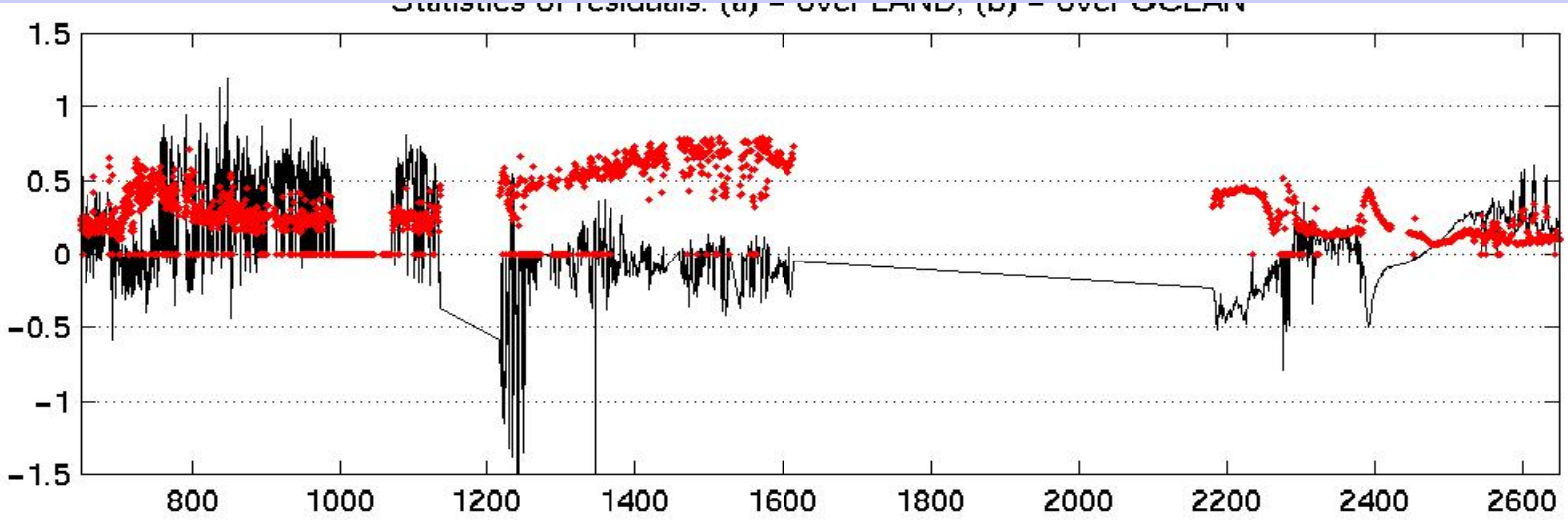

b

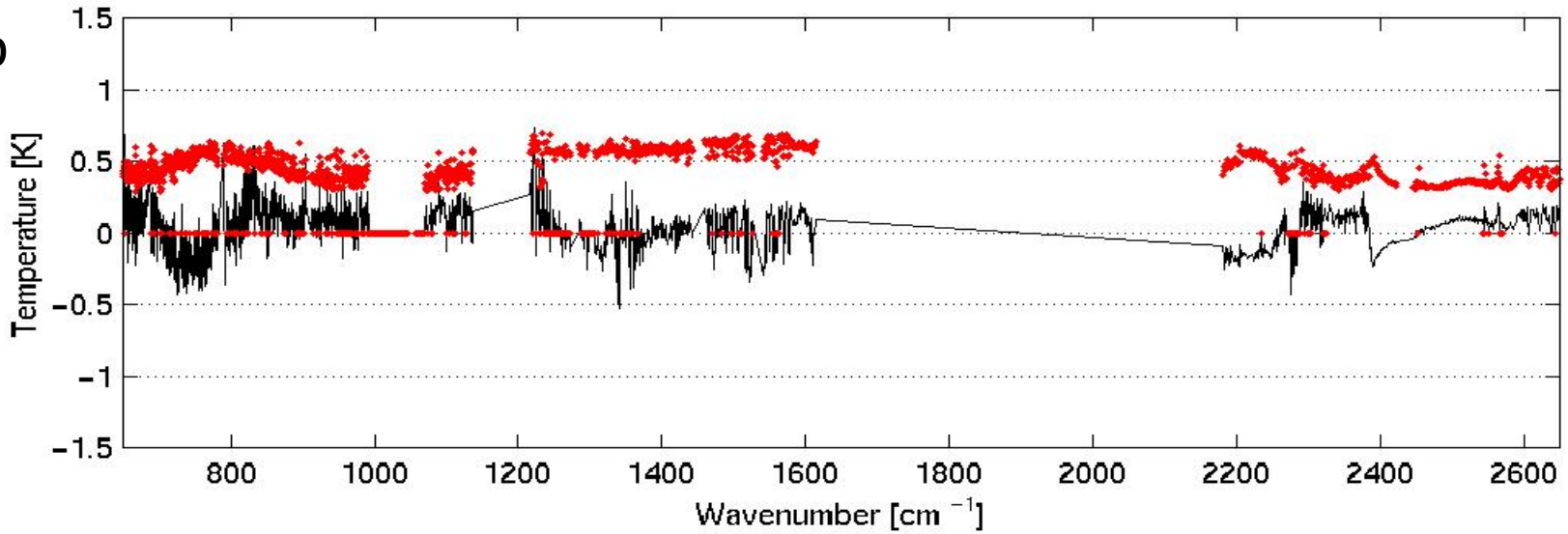

Conclusion: Analysis of measurements show that:

The spatial smoothing technique is effective for filtering the SW spatial component of measurement errors; smoothed spatial fields of radiances correspond better to the spatial properties of the desired spatial fields of atmospheric temperature-moisture profiles.

Non-blackbody surface emissivity significantly weakens the radiance signal and has strong influence on lower tropospheric temperature and moisture retrievals

ε_{IR}(sfc) presents strong spectral and spatial variability over land surfaces;

Solutions with ε_{IR}(sfc) consideration are improving the vertical-horizontal spatial structure of atmospheric temperature-moisture estimates